

The Landscape of the Hubbard Model

Subir Sachdev

Department of Physics, Harvard University, Cambridge MA 02138

(Dated: October 17, 2019)

Abstract

I present a pedagogical survey of a variety of quantum phases of the Hubbard model. The honeycomb lattice model has a conformal field theory connecting the semi-metal to the insulator with Néel order. States with fractionalized excitations are linked to the deconfined phases of gauge theories. I also consider the confining phases of such gauge theories, and show how Berry phases of monopoles induce valence bond solid order. Compressible metallic phases with Fermi surfaces are described, including the ‘fractionalized Fermi liquid’, using the Hubbard model on a bilayer triangular lattice. I make numerous connections to the AdS/CFT correspondence, reviewing insights gained and discussing open problems that the correspondence could address.

TASI (Boulder, June 2010) and Chandrasekhar (Bangalore, Dec 2010) lectures.

I. INTRODUCTION

The Hubbard model is the simplest of a class of models describing electrons moving on a lattice with repulsive electron-electron interactions. Despite its apparent simplicity, it has become clear in the past two decades that it can display a very rich phase diagram, with a plethora of interesting phases. The most common phase is, of course, the Fermi liquid (FL), which is adiabatically connected to the metallic phase of non-interacting electrons. However, electron-electron interactions can break one or more symmetries of the Hamiltonian, and this leads to phases such as antiferromagnets, charge or spin density waves, or superconductors. Also of great interest are quantum phases which do not break any symmetries, but are nevertheless qualitatively distinct from the non-interacting electron states: such states are characterized by emergent gauge excitations, fractionalization of quasiparticle excitations, and non-trivial ground state degeneracies which depend upon the global topology of the lattice—it is often stated that such states have ‘topological’ order. Finally, there are interesting quantum phase transitions between such phases, and such quantum critical points are often described by strongly-coupled quantum field theories. In some cases, the quantum critical points can broaden into gapless quantum critical phases.

This article will present a pedagogical review of a small sample of this landscape of phases and critical points. My aim is to describe the appearance of a variety of non-trivial phases in the simplest possible context. For the honeycomb lattice with a density of one electron per site, such phases naturally have low energy excitations which have a relativistic form at low energies. Consequently, in the vicinity of quantum phase transitions, such phases and their critical points are amenable to a description by relativistic quantum field theories. In some cases, the critical points are also conformally invariant, and so are described by conformal field theories (CFTs). In these cases, the AdS/CFT correspondence can be directly applied, and I will describe the insights that have been gained from such an approach.

However, once we move away from commensurate electron densities, the quantum phases and critical points of electron lattice models rarely have any relativistic invariance in their low energy theory. I will describe here the simplest examples of ‘topologically ordered’ phases at generic electron densities. It is important to note that the lack of relativistic invariance does not rule out application of the AdS/CFT correspondence. We can begin from a relativistically invariant gravity dual theory and dope it with charge carriers by turning on a chemical potential: then even the gravity theory is not relativistically invariant at low energies, and we can hope to match its low energy physics to a condensed matter system. There has been a large effort to apply the AdS/CFT correspondence along this direction in the past few years. I have discussed some of this work in another recent review article¹, which should be viewed as a complement to the present article. I will also discuss the generic density phases here, with an emphasis on the general low energy structure of the ‘fractionalized Fermi liquid’ (FL*) phase^{2,3}, which I believe is closely related to the generic density phases that have appeared using the AdS/CFT correspondence⁴.

I begin by introducing the Hubbard model. It is defined by the Hamiltonian

$$H = - \sum_{i,j} t_{ij} c_{i\alpha}^\dagger c_{j\alpha} + \sum_i \left[-\mu (n_{i\uparrow} + n_{i\downarrow}) + U_i \left(n_{i\uparrow} - \frac{1}{2} \right) \left(n_{i\downarrow} - \frac{1}{2} \right) \right]. \quad (1.1)$$

Here $c_{i\alpha}$, $\alpha = \uparrow, \downarrow$ are annihilation operators on the site i of a regular lattice, and t_{ij} is a Hermitian, short-range matrix containing the ‘hopping matrix elements’ which move the electrons between different lattice sites. The density of electrons is controlled by the chemical potential μ which couples to the total electron density, with

$$n_{i\uparrow} \equiv c_{i\uparrow}^\dagger c_{i\uparrow} \quad , \quad n_{i\downarrow} \equiv c_{i\downarrow}^\dagger c_{i\downarrow}. \quad (1.2)$$

The electrons repel each other with an on-site interaction U_i ; in most cases we will take $U_i = U$ site-independent, but it will also be useful later to allow for a site-dependent U_i . For completeness, we also note the algebra of the fermion operators:

$$\begin{aligned} c_{i\alpha} c_{j\beta}^\dagger + c_{j\beta}^\dagger c_{i\alpha} &= \delta_{ij} \delta_{\alpha\beta} \\ c_{i\alpha} c_{j\beta} + c_{j\beta} c_{i\alpha} &= 0. \end{aligned} \quad (1.3)$$

The equations (1.1), (1.2), and (1.3) constitute a self-contained and complete mathematical statement of the problem of the landscape of the Hubbard model. It is remarkable that a problem that is so simple to state has such a rich phase structure as a function of the lattice choice, the fermion density, and the spatial forms of t_{ij} and U_i .

Sections II, IV, and V will deal exclusively with the honeycomb lattice at a density of one electron per site (“half-filling”), so that $\langle n_{i\uparrow} \rangle = \langle n_{i\downarrow} \rangle = 1/2$. The emphasis on the honeycomb lattice is not motivated by its particular physical importance (although, it is the lattice of graphene), but by its simplicity as a context for introducing various technical methods, quantum phases and critical points. In Section II, we will consider the semi-metal and the insulating antiferromagnet, and show that a phase transition between them is described by a relativistic field theory, which is a version of the Gross-Neveu-Yukawa model; Section III will use this field theory to present a general discussion of the physics at non-zero temperatures in the vicinity of a quantum critical point. We will focus on the transport of conserved charges, and describe insights gained from the AdS/CFT correspondence. Section IV will consider the problem of restoring the spin rotation symmetry from the antiferromagnet, while remaining in an insulating phase: this will lead to a description in terms of a U(1) gauge theory, and the appearance of an insulating phase with valence bond solid (VBS) order. Finally, Section V will combine all the phases of the half-filled honeycomb lattice discussed so far in a single phase diagram: this will require introduction of a SU(2) gauge theory. We will find an interesting multi-critical point in Section V, which has many features in common with the supersymmetric CFTs studied using the AdS/CFT correspondence.

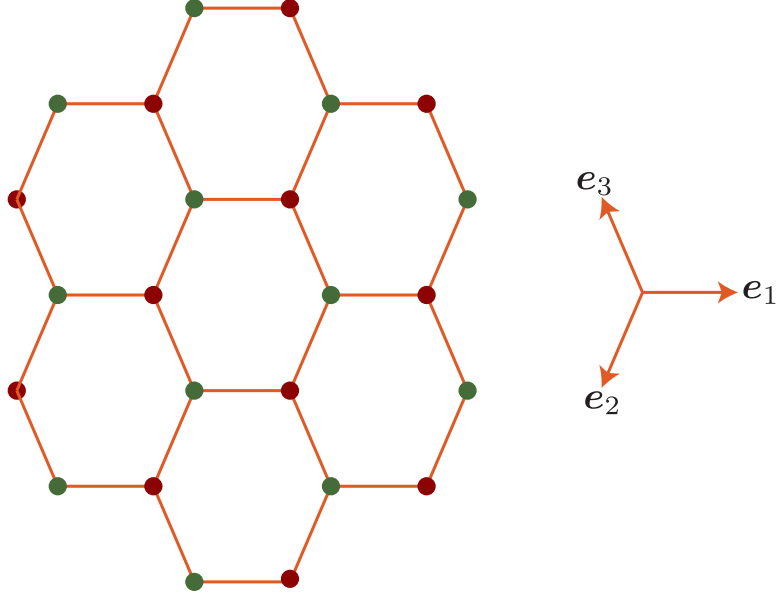


FIG. 1: The honeycomb lattice with its A (green) and B (red) sublattices

We will move away from half-filling in Section VI, where we will turn our attention to metallic phases with Fermi surfaces. Here we will use the Hubbard model on a bilayer triangular lattice, which has been realized in experiments⁵ on ^3He . We will present a gauge theory whose phases include the Fermi liquid (FL) and the fractionalized Fermi liquid (FL*).

II. SEMI-METAL AND ANTIFERROMAGNETISM ON THE HONEYCOMB LATTICE

A. Preliminaries

We will consider the Hubbard model (1.1) with the sites i on locations \mathbf{r}_i on the honeycomb lattice shown in Fig. 1. Here, we set up some notation allowing us to analyze the geometry of this lattice.

We work with a lattice with unit nearest neighbor spacing. We define unit length vectors which connect nearest-neighbor sites

$$\mathbf{e}_1 = (1, 0) \quad , \quad \mathbf{e}_2 = (-1/2, \sqrt{3}/2) \quad , \quad \mathbf{e}_3 = (-1/2, -\sqrt{3}/2). \quad (2.1)$$

Note that $\mathbf{e}_i \cdot \mathbf{e}_j = -1/2$ for $i \neq j$, and $\mathbf{e}_1 + \mathbf{e}_2 + \mathbf{e}_3 = 0$. The lattice can be divided into the A and B sublattices, as shown in Fig. 1. We take the origin of co-ordinates of the lattice at the center of an *empty hexagon*. The A sublattice sites closest to the origin are at \mathbf{e}_1 , \mathbf{e}_2 , and \mathbf{e}_3 , while the B sublattice sites closest to the origin are at $-\mathbf{e}_1$, $-\mathbf{e}_2$, and $-\mathbf{e}_3$.

The unit cell of the hexagonal lattice contains 2 sites, one each from the A and B sub-

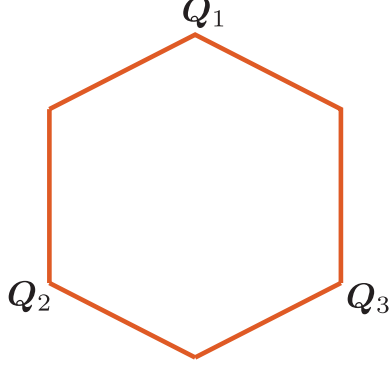


FIG. 2: The first Brillouin zone of the honeycomb lattice.

lattices. These unit cells form a triangular Bravais lattice consisting of the centers of the hexagons. The triangular lattice points closest to the origin are $\pm(\mathbf{e}_1 - \mathbf{e}_2)$, $\pm(\mathbf{e}_2 - \mathbf{e}_3)$, and $\pm(\mathbf{e}_3 - \mathbf{e}_1)$. The reciprocal lattice is a set of wavevectors \mathbf{G} such that $\mathbf{G} \cdot \mathbf{r} = 2\pi \times \text{integer}$, where \mathbf{r} is the center of any hexagon of the honeycomb lattice. The reciprocal lattice is also a triangular lattice, and it consists of the points $\sum_i n_i \mathbf{G}_i$, where n_i are integers and

$$\mathbf{G}_1 = \frac{4\pi}{3}\mathbf{e}_1 \quad , \quad \mathbf{G}_2 = \frac{4\pi}{3}\mathbf{e}_2 \quad , \quad \mathbf{G}_3 = \frac{4\pi}{3}\mathbf{e}_3. \quad (2.2)$$

The unit cell of the reciprocal lattice is called the first Brillouin zone. This is a hexagon whose vertices are given by

$$\mathbf{Q}_1 = \frac{1}{3}(\mathbf{G}_2 - \mathbf{G}_3) \quad , \quad \mathbf{Q}_2 = \frac{1}{3}(\mathbf{G}_3 - \mathbf{G}_1) \quad , \quad \mathbf{Q}_3 = \frac{1}{3}(\mathbf{G}_1 - \mathbf{G}_2), \quad (2.3)$$

and $-\mathbf{Q}_1$, $-\mathbf{Q}_2$, and $-\mathbf{Q}_3$; see Fig. 2. Integrals and sums over momentum space will implicitly extend only over the first Brillouin zone. This is the ‘ultraviolet cutoff’ imposed by the underlying lattice structure.

We define the Fourier transform of the electrons on the A sublattice by

$$c_{A\alpha}(\mathbf{k}) = \frac{1}{\sqrt{\mathcal{N}}} \sum_{i \in A} c_{i\alpha} e^{-i\mathbf{k} \cdot \mathbf{r}_i}, \quad (2.4)$$

where \mathcal{N} is the number of sites on one sublattice; similarly for $c_{B\alpha}$. Note that $c_{A\alpha}(\mathbf{k} + \mathbf{G}) = c_{A\alpha}(\mathbf{k})$: consequently, sums over momentum have to be restricted to the first Brillouin zone to avoid double counting. Thus the inverse of Eq. (2.4) sums over \mathbf{k} in the first Brillouin zone.

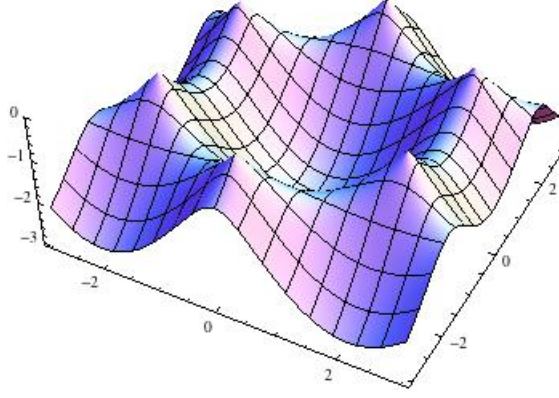


FIG. 3: The lower band of the dispersion in Eq. (2.7 for $\mu = 0$

B. Semi-metal

We begin with free electrons in the honeycomb lattice, $U = 0$, with only nearest-neighbor electron hopping $t_{ij} = t$. Using Eq. (2.4), we can write the hopping Hamiltonian as

$$H_0 = -t \sum_{\mathbf{k}} \left(e^{i\mathbf{k} \cdot \mathbf{e}_1} + e^{i\mathbf{k} \cdot \mathbf{e}_2} + e^{i\mathbf{k} \cdot \mathbf{e}_3} \right) c_{A\alpha}^\dagger(\mathbf{k}) c_{B\alpha}(\mathbf{k}) + \text{H.c.} \\ - \mu \sum_{\mathbf{k}} \left(c_{A\alpha}^\dagger(\mathbf{k}) c_{A\alpha}(\mathbf{k}) + c_{B\alpha}^\dagger(\mathbf{k}) c_{B\alpha}(\mathbf{k}) \right) \quad (2.5)$$

We introduce Pauli matrices τ^a ($a = x, y, z$) which act on the A, B sublattice space; then this Hamiltonian can be written as

$$H_0 = \sum_{\mathbf{k}} c^\dagger(\mathbf{k}) \left[-\mu - t \left(\cos(\mathbf{k} \cdot \mathbf{e}_1) + \cos(\mathbf{k} \cdot \mathbf{e}_2) + \cos(\mathbf{k} \cdot \mathbf{e}_3) \right) \tau^x \right. \\ \left. + t \left(\sin(\mathbf{k} \cdot \mathbf{e}_1) + \sin(\mathbf{k} \cdot \mathbf{e}_2) + \sin(\mathbf{k} \cdot \mathbf{e}_3) \right) \tau^y \right] c(\mathbf{k}), \quad (2.6)$$

where the sublattice and spin indices on the electrons are now implicit: the $c(\mathbf{k})$ are 4-component fermion operators.

The energy eigenvalues are easily determined to be

$$-\mu \pm \left| e^{i\mathbf{k} \cdot \mathbf{e}_1} + e^{i\mathbf{k} \cdot \mathbf{e}_2} + e^{i\mathbf{k} \cdot \mathbf{e}_3} \right| \quad (2.7)$$

and these are plotted in Fig. 3. At half-filling, exactly half the states should be occupied in the ground state, and for the spectrum in Eq. (2.7) this is achieved at $\mu = 0$.

A crucial feature of any metallic state is the Fermi surface: this is boundary between the occupied and empty states in momentum space. In two spatial dimensions, this boundary is generically a line in momentum space, and this is the case for the dispersion in Eq. (2.7)

for $\mu \neq 0$. However, for the $\mu = 0$, the honeycomb lattice has the special property that the occupied and empty states meet only at a discrete set of single points in momentum space: this should be clear from the dispersion plotted in Fig. 3. Only 2 of these points are distinct, in that they are not separated by a reciprocal lattice vector \mathbf{G} . So the half-filled honeycomb lattice has 2 ‘Fermi points’, and realizes a ‘semi-metal’ phase. The low energy excitations of the semi-metal consist of particles and holes across the Fermi point, and these have a lower density of states than in a metallic phase with a Fermi line. We also note that the Fermi-point structure is protected by a sublattice exchange symmetry: it is not special to the nearest-neighbor hopping model, and it also survives the inclusion of electron-electron interactions.

We obtain a very useful, and universal, theory for the low energy excitations of the semi-metal by expanding (2.6) in the vicinity of the Fermi points. The distinct Fermi points are present at \mathbf{Q}_1 and $-\mathbf{Q}_1$; all other Fermi points are separated from these two points by a reciprocal lattice vector \mathbf{G} . So we define continuum Fermi field which reside in ‘valleys’ in the vicinity of these points by

$$\begin{aligned} C_{A1\alpha}(\mathbf{k}) &= \sqrt{A} c_{A\alpha}(\mathbf{Q}_1 + \mathbf{k}) \\ C_{A2\alpha}(\mathbf{k}) &= \sqrt{A} c_{A\alpha}(-\mathbf{Q}_1 + \mathbf{k}) \\ C_{B1\alpha}(\mathbf{k}) &= \sqrt{A} c_{B\alpha}(\mathbf{Q}_1 + \mathbf{k}) \\ C_{B2\alpha}(\mathbf{k}) &= \sqrt{A} c_{B\alpha}(-\mathbf{Q}_1 + \mathbf{k}), \end{aligned} \quad (2.8)$$

where A is the total area of the honeycomb lattice, and the momentum \mathbf{k} is small. The field C is a 8-component continuum canonical Fermi field: the components correspond to spin (\uparrow, \downarrow), sublattice (A, B), and valley (1, 2) indices. We will also use Pauli matrices which act on the spin (σ^a), sublattice (τ^a), and valley (ρ^a) space.

Inserting Eq. (2.8) into Eq. (2.6), we obtain the continuum Hamiltonian

$$H_0 = \int \frac{d^2k}{4\pi^2} C^\dagger(\mathbf{k}) \left(v\tau^y k_x + v\tau^x \rho^z k_y \right) C(\mathbf{k}), \quad (2.9)$$

where $v = 3t/2$. From now on we rescale time to set $v = 1$. Diagonalizing Eq. (2.9), we obtain the relativistic spectrum

$$\pm \sqrt{k_x^2 + k_y^2}, \quad (2.10)$$

which corresponds to the values of Eq. (2.7) near the Fermi points.

The relativistic structure of H_0 can be made explicit by rewriting it as the Lagrangian of massless Dirac fermions. Define $\bar{C} = C^\dagger \rho^z \tau^z$. Then we can write the Euclidean time (τ) Lagrangian density of the semi-metal phase as

$$\mathcal{L}_0 = \bar{C} (\partial_\tau \gamma_0 + \partial_x \gamma_1 + \partial_y \gamma_2) C \quad (2.11)$$

where ω is the frequency associated with imaginary time, and the Dirac γ matrices are

$$\gamma_0 = -\rho^z \tau^z \quad \gamma_1 = \rho^z \tau^x \quad \gamma_2 = -\tau^y. \quad (2.12)$$

In addition to relativistic invariance, this form makes it clear the free-fermion Lagrangian has a large group of ‘flavor’ symmetries that acts on the 8×8 fermion space and commute with the γ matrices. Most of these symmetries are not obeyed by higher-order gradients, or by fermion interaction terms which descend from the Hubbard model.

Let us now turn on a small repulsion, U , between the fermions in the semi-metal. Because of the point-like nature of the Fermi surface, it is easier to determine the consequences of this interaction here than in a metallic phase with a Fermi line of gapless excitations. We can use traditional renormalization group (RG) methods to conclude that a weak U is irrelevant in the infrared: the computation is left as an exercise below. Consequently, the semi-metal state is a stable phase which is present over a finite range of parameters.

Exercise: Observe that \mathcal{L}_0 is invariant under the scaling transformation $x' = xe^{-\ell}$ and $\tau' = \tau e^{-\ell}$. Write the Hubbard interaction U in terms of the Dirac fermions, and show that it has the tree-level scaling transformation $U' = Ue^{-\ell}$. So argue that all short-range interactions are *irrelevant* in the Dirac semi-metal phase.

C. Antiferromagnet

Although a small U is irrelevant, new phases can and do appear at large U . To see this, let us return to the lattice Hubbard model in Eq. (1.1), and consider the limit of large $U_i = U$. We will assume $\mu = 0$ and half-filling in the remainder of this section.

At $U = \infty$, the eigenstates are simple products over the states on each site. Each site has 4 states:

$$|0\rangle \quad , \quad c_{i\uparrow}^\dagger |0\rangle \quad , \quad c_{i\downarrow}^\dagger |0\rangle \quad , \quad c_{i\uparrow}^\dagger c_{i\downarrow}^\dagger |0\rangle, \quad (2.13)$$

where $|0\rangle$ is the empty state. The energies of these states are $U/4$, $-U/4$, $-U/4$, and $U/4$ respectively. Thus the ground state on each site is doubly-degenerate, corresponding to the spin-up and spin-down states of a single electron. The lattice model has a degeneracy of $2^{2\mathcal{N}}$, and so a non-zero entropy density (recall that \mathcal{N} is the number of sites on one sublattice).

Any small perturbation away from the $U = \infty$ limit is likely to lift this exponential large degeneracy. So we need to account for the electron hopping t . At first order, electron hopping moves an electron from one singly-occupied site to another, yielding a final state with one empty and one doubly occupied site. This final state has an energy U higher than the initial state, and so is not part of the low energy manifold. So by the rules of degenerate perturbation theory, there is no correction to the energy of all the $2^{2\mathcal{N}}$ ground states at first order in t .

At second order in t , we have to use the effective Hamiltonian method. This performs a canonical transformation to eliminate the couplings from the ground states to all the states excited by energy U , while obtaining a modified Hamiltonian which acts on the 2^{2N} ground states. This method is described in text books on quantum mechanics, and we leave its application here as an exercise. The resulting effective Hamiltonian is the Heisenberg antiferromagnet:

$$H_J = \sum_{i<j} J_{ij} S_i^a S_j^a \quad , \quad J_{ij} = \frac{4t_{ij}^2}{U}, \quad (2.14)$$

where J_{ij} is the exchange interaction and S_i^a are the spin operators on site i

$$S_i^a = \frac{1}{2} c_{i\alpha}^\dagger \sigma_{\alpha\beta}^a c_{i\beta}. \quad (2.15)$$

Note that these spin operators preserve the electron occupation number on every site, and so act within the subspace of the 2^{2N} low energy states. The Hamiltonian H_J lifts the macroscopic degeneracy, and the entropy density of the new ground state will be zero.

Exercise: Use the effective Hamiltonian method described in Ref. 6 to obtain Eq. (2.14). At second order in U , it is sufficient to consider the 2-site Hubbard model. This has a total of 16 states, and 4 ground states at $U = \infty$. Derive the effective Hamiltonian which acts on these 4 states at order t^2 .

Although we cannot compute the exact ground state of H_J on the honeycomb lattice with nearest-neighbor exchange, numerical studies⁷ leave little doubt to its basic structure. The ground state is adiabatically connected to that obtained by treating the S_i^a as classical vectors in spin space: it has antiferromagnetic (or Néel) order which breaks the global SU(2) spin rotation symmetry, by a spontaneous polarization of the spins on opposite orientations on the two sublattices

$$\eta_i \langle S_i^a \rangle = N^a, \quad (2.16)$$

where $\eta_i = 1$ ($\eta_i = -1$) on sublattice A (B), and N^a is the vector Néel order parameter. Classically this state minimizes the exchange coupling in Eq. (2.14) because $J_{ij} > 0$. Quantum fluctuations for spin $S = 1/2$ reduce the spontaneous moment from its classical value, but a non-zero moment remains on the honeycomb lattice.

What is the electronic excitation spectrum in the antiferromagnet? To determine this, it is useful to write the Néel order parameter in terms of the continuum Dirac fields introduced in Section II B. We observe

$$\sum_i \eta_i S_i^a = \sum_{\mathbf{k}} \left(c_{A\alpha}^\dagger \sigma_{\alpha\beta}^a c_{A\beta} - c_{B\alpha}^\dagger \sigma_{\alpha\beta}^a c_{B\beta} \right) = \int \frac{d^2 k}{4\pi^2} C^\dagger \tau^z \sigma^a C \quad (2.17)$$

Thus the Néel order parameter N^a is given by the fermion bilinear

$$N^a = \langle C^\dagger \tau^z \sigma^a C \rangle = \langle \bar{C} \rho^z \sigma^a C \rangle, \quad (2.18)$$

and the vacuum expectation value (VEV) is non-zero in the antiferromagnet. We can expect that electron-electron interactions will induce a coupling between the fermion excitations and this VEV in the low energy Hamiltonian for the Néel phase. Choosing Néel ordering in the z direction

$$N^a = N_0 \delta_{az}, \quad (2.19)$$

we anticipate that H_0 in Eq. (2.9) is modified in the Néel phase to

$$H_N = \int \frac{d^2 k}{4\pi^2} C^\dagger(\mathbf{k}) \left(\tau^y k_x + \tau^x \rho^z k_y - \lambda N_0 \tau^z \sigma^z \right) C(\mathbf{k}), \quad (2.20)$$

where λ is a coupling determined by the electron interactions, and we have assumed Néel order polarized in the z direction. This effective Hamiltonian will be explicitly derived in the next subsection. We can now easily diagonalize H_N to deduce that the electronic excitations have energy

$$\pm \sqrt{k_x^2 + k_y^2 + \lambda^2 N_0^2} \quad (2.21)$$

. This is the spectrum of massive Dirac fermions. So the Fermi point has disappeared, and an energy gap has opened in the fermion excitation spectrum. In condensed matter language, the phase with antiferromagnetic order is an insulator, and not a semi-metal: transmission of electronic charge will require creation of gapped particle and hole excitations.

D. Quantum phase transition

We have now described a semi-metal phase for small U , and an antiferromagnetic insulator for large U . Both are robust phases, whose existence has been reliably established. We now consider connecting these two phases at intermediate values of U . This is a complex subject, and careful numerical studies are only just emerging for the model with nearest-neighbor hopping⁷. It is already clear, however, that by varying the form of the microscopic coupling we can obtain a rich variety of intermediate phases^{8–13}. In the present subsection we consider the simplest possibility: there are no new intermediate phases, and only a direct quantum phase transition between the semi-metal and the antiferromagnetic insulator^{14–16}.

We can derive the field theory for this direct transition either by symmetry considerations, or by an explicit derivation from the Hubbard model. Let us initially follow the second route. We start with the Hubbard Hamiltonian in Eq. (1.1), use the operator identity (valid on each site i):

$$U \left(n_\uparrow - \frac{1}{2} \right) \left(n_\downarrow - \frac{1}{2} \right) = -\frac{2U}{3} S^{a2} + \frac{U}{4}. \quad (2.22)$$

Then, in the fermion coherent state path integral for the Hubbard model, we apply a ‘Hubbard-Stratonovich’ transformation to the interaction term; this amounts to using the identity

$$\begin{aligned} & \exp \left(\frac{2U}{3} \sum_i \int d\tau S_i^{a2} \right) \\ &= \int \mathcal{D}X_i^a(\tau) \exp \left(- \sum_i \int d\tau \left[\frac{3}{8} X_i^{a2} - \sqrt{U} X_i^a S_i^a \right] \right) \end{aligned} \quad (2.23)$$

The fermion path integral is now a bilinear in the fermions, and we can, at least formally, integrate out the fermions in the form of a functional determinant. We imagine doing this temporarily, and then look for the saddle point of the resulting effective action for the X_i^a . At the saddle-point we find that the lowest energy is achieved when the vector has opposite orientations on the A and B sublattices. Anticipating this, we look for a continuum limit in terms of a field φ^a where

$$X_i^a = \eta_i \varphi^a \quad (2.24)$$

Using Eq. (2.17), the continuum limit of the coupling between the field φ^a and the fermions in Eq. (2.23) is given by

$$X_i^a c_{i\alpha}^\dagger \sigma_{\alpha\beta}^a c_{i\beta} = \varphi^a C^\dagger \tau^z \sigma^a C = \varphi^a \bar{C} \rho^z \sigma^a C \quad (2.25)$$

From this it is clear that φ^a is a dynamical quantum field which represents the fluctuations of the local Néel order, and

$$\langle \varphi^a \rangle \propto N^a. \quad (2.26)$$

Now we can take the continuum limit of all the terms in the coherent state path integral for the lattice Hubbard model and obtain the following continuum Lagrangian density

$$\mathcal{L} = \bar{C} \gamma_\mu \partial_\mu C + \frac{1}{2} [(\partial_\mu \varphi^a)^2 + s \varphi^{a2}] + \frac{u}{24} (\varphi^{a2})^2 - \lambda \varphi^a \bar{C} \rho^z \sigma^a C \quad (2.27)$$

This is a relativistic quantum field theory for the 8-component fermion field C and the 3-component real scalar φ^a , related to the Gross-Neveu-Yukawa model. We have included gradient terms and quartic in the Lagrangian for φ^a : these are not present in the derivation outlined above from the lattice Hubbard model, but are clearly induced by higher energy fermions are integrated out. The Lagrangian includes various phenomenological couplings constants (s, u, λ); as these constants are varied, \mathcal{L} can describe *both* the semi-metal and insulating antiferromagnet phases, and also the quantum critical point between them.

Note that the matrix $\rho^z \sigma^a$ commutes with all the γ_μ ; hence $\rho^z \sigma^a$ is a matrix in “flavor” space. So if we consider C as 2-component Dirac fermions, then these Dirac fermions carry an additional 4-component flavor index.

The semi-metal phase is the one where φ^a has vanishing VEV. In mean-field theory, this appears for $s > 0$. The φ^a excitations are then massive, and these constitute a triplet of gapped ‘spin-excitons’ associated with fluctuations of the local antiferromagnetic order. The Dirac fermions are massless, and represent the Fermi point excitations of the semi-metal.

The Néel phase has a non-zero VEV, $\langle \varphi^a \rangle \neq 0$, and appears in mean-field theory for $s < 0$. Here the Dirac fermions acquire a gap, indicating that the Fermi point has vanished, and we are now in an insulating phase. The fluctuations of φ are a doublet of Goldstone modes (‘spin waves’) and a longitudinal massive Higgs boson.

Finally, we are ready to address the quantum critical point between these phases. In mean-field theory, this transition occurs at $s = 0$. As is customary in condensed matter physics, it is useful to carry out an RG analysis near this point. The tree-level analysis is carried out in the following exercise.

Exercise: Perform a tree-level RG transformation on \mathcal{L} . The quadratic gradient terms are invariant under $C' = Ce^\ell$ and $\varphi' = \varphi e^{\ell/2}$. Show that this leads to $s' = se^{2\ell}$. Thus s is a relevant perturbation which drives the system into either the semi-metal or antiferromagnetic insulator. The quantum critical point is reached by tuning s to its critical value ($= 0$ at tree level). Show that the couplings u and λ are both relevant perturbations at this critical point. Thus, while interactions are irrelevant in the Dirac semi-metal (and in the insulator), they are strongly relevant at the quantum-critical point.

Further study of this quantum critical point requires a RG analysis which goes beyond tree-level. Such an analysis can be controlled in an expansion in $1/N$ (where N is the number of fermion flavors) or $(3-d)$ (where d is the spatial dimensionality. For reviews see Ref. 17 or Chapter 17 of Ref. 18. The main conclusion of such analyses is that there is an RG fixed point at which the φ^{a2} is the only relevant perturbation. Non-linearities such as λ and u all reach stable fixed point values of order unity. This non-trivial fixed point implies that the physics of the quantum critical point is highly non-trivial and strongly coupled.

We will not describe the critical theory in any detail here. However, we will note some important characteristics of correlation functions at the quantum critical point. The electron Green’s function has the following structure

$$\langle C(k, \omega); C^\dagger(k, \omega) \rangle \sim \frac{i\omega + k_x \tau^y + k_y \tau^x \rho^z}{(\omega^2 + k_x^2 + k_y^2)^{1-\eta/2}} \quad (2.28)$$

where $\eta > 0$ is the *anomalous dimension* of the fermion. This leads to a fermion spectral density which has no quasiparticle pole: thus the quantum critical point has no well-defined quasiparticle excitations. This distinguishes it from both the semi-metal and insulating antiferromagnetic phases that flank it on either side: both had excitations with infinitely-sharp quasiparticle peaks. Similar anomalous dimensions appear in the correlations of the bosonic order parameter φ^a .

E. Electrical transport

An important set of observables which do *not* acquire anomalous dimensions at the quantum critical point are the currents associated with global conservation laws. As the simplest example here, let us consider correlations of the conserved electric charge of the electrons, and the associated electrical conductivity σ . At zero temperature ($T = 0$), we have $\sigma = 0$ in the insulator, while the semi-metal and the quantum critical point have finite non-zero values of σ , as we will now see.

The conserved electrical current is

$$J_\mu = -i\bar{C}\gamma_\mu C. \quad (2.29)$$

Let us compute its two-point correlator, $K_{\mu\nu}(k)$ at a spacetime momentum k_μ . At leading order, this is given by a one fermion loop diagram which evaluates to

$$\begin{aligned} K_{\mu\nu}(k) &= \int \frac{d^3p}{8\pi^3} \frac{\text{Tr}[\gamma_\mu(i\gamma_\lambda p_\lambda + m\rho^z\sigma^z)\gamma_\nu(i\gamma_\delta(k_\delta + p_\delta) + m\rho^z\sigma^z)]}{(p^2 + m^2)((p+k)^2 + m^2)} \\ &= -\frac{2}{\pi} \left(\delta_{\mu\nu} - \frac{k_\mu k_\nu}{k^2} \right) \int_0^1 dx \frac{k^2 x(1-x)}{\sqrt{m^2 + k^2 x(1-x)}}, \end{aligned} \quad (2.30)$$

where the mass $m = 0$ in the semi-metal and at the quantum critical point, while $m = |\lambda N_0|$ in the insulator. Note that the current correlation is purely transverse, and this follows from the requirement of current conservation

$$k_\mu K_{\mu\nu} = 0. \quad (2.31)$$

Of particular interest to us is the K_{00} component, after analytic continuation to Minkowski space where the spacetime momentum k_μ is replaced by (ω, k) . The conductivity is obtained from this correlator via the Kubo formula

$$\sigma(\omega) = \lim_{k \rightarrow 0} \frac{-i\omega}{k^2} K_{00}(\omega, k). \quad (2.32)$$

In the insulator, where $m > 0$, analysis of the integrand in Eq. (2.30) shows that the spectral weight of the density correlator has a gap of $2m$ at $k = 0$, and the conductivity in Eq. (2.32) vanishes. These properties are as expected in any insulator.

In the metal, and at the critical point, where $m = 0$, the fermionic spectrum is gapless, and so is that of the charge correlator. The density correlator in Eq. (2.30) and the conductivity

in Eq. (2.32) evaluate to the simple universal results

$$\begin{aligned} K_{00}(\omega, k) &= \frac{1}{4} \frac{k^2}{\sqrt{k^2 - \omega^2}} \\ \sigma(\omega) &= \frac{1}{4}. \end{aligned} \tag{2.33}$$

How about beyond the one-loop results? The insulator maintains a gap to charged excitations, and so the conductivity remains at zero. In the semi-metal, the fermions are gapless, but they couple only to the gapped fluctuations of the Néel order φ^a . Examination of the perturbation theory shows that these have no effect on the current correlators at small momenta and frequency, and so the results in Eq. (2.33) are *exact* in the limit of small ω and k in the semi-metal.

At the quantum critical point, we have to consider the strong critical fluctuations associated with fixed-point values of the Yukawa coupling λ and the quartic bosonic interaction u . These can be examined in the $(3-d)$ or the $1/N$ expansion, and require evaluation of multi-loop diagrams. We will not describe the computations here, but note a remarkable feature: all divergences associated with the critical fluctuations cancel, and the final result is universal. The values of none of the couplings of the Lagrangian in Eq. (2.27) matters because these are all pinned by the RG fixed point. There are no anomalous dimensions, and the results in Eq. (2.33) generalize to

$$\begin{aligned} K_{00}(\omega, k) &= \mathcal{K} \frac{k^2}{\sqrt{k^2 - \omega^2}} \\ \sigma(\omega) &= \mathcal{K}, \end{aligned} \tag{2.34}$$

where \mathcal{K} is a universal number dependent only upon the universality class of the quantum critical point. The value of the \mathcal{K} for the Gross-Neveu-Yukawa model in Eq. (2.27) is not known exactly, but can be estimated by computations in the $(3-d)$ or $1/N$ expansions.

III. NON-ZERO TEMPERATURES AND THE ADS/CFT CORRESPONDENCE

We begin by some general remarks on the influence of a non-zero temperature, T , on a generic, strongly-coupled quantum critical point. Let us consider a quantum-critical point which has only a single relevant perturbation, s , as is the case for the model in Eq. (2.27) (the generalization to several relevant perturbations is immediate). So near the quantum critical point, the RG flow is described by

$$\frac{ds}{d\ell} = \frac{1}{\nu} s. \tag{3.1}$$

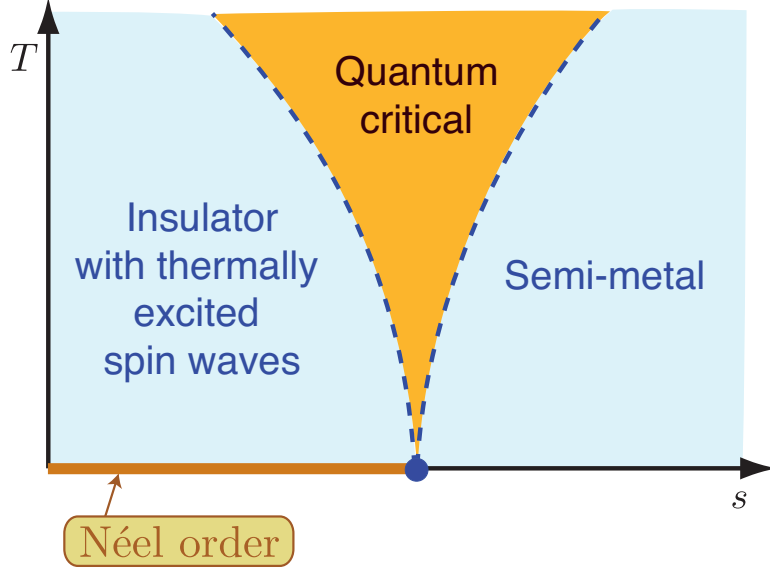


FIG. 4: Canonical quantum critical crossover phase diagram. The dashed lines occur for $T \sim |s|^{z\nu}$, and indicate crossovers between the orange- and blue-shaded regions which are generic from any strongly-coupled quantum critical point. Specific features of the blue-shaded regions for the theory Eq. (2.27) of the transition from the semi-metal to the Néel-ordered insulator are also indicated. The Néel order vanishes for any $T > 0$ because non-Abelian continuous symmetries cannot be broken in two spatial dimensions.

In standard condensed matter notation, the eigenvalue of the relevant flow is written in terms of ν , the correlation length exponent. Now in the quantum field theory in Euclidean time, a non-zero T corresponds to placing the theory on a cylinder of circumference $1/T$. Such a finite size is clearly relevant in the infrared, and also indicates that $1/T$ transforms just like the temporal length under the RG. We write this as

$$\frac{dT}{d\ell} = zT, \quad (3.2)$$

where z is the dynamic critical exponent. All the theories for the honeycomb lattice at half filling have $z = 1$, but we allow z to be arbitrary here.

Eqs. (3.1) and (3.2) are of course trivial to integrate

$$s(\ell) = se^{\ell/\nu} \quad , \quad T(\ell) = Te^{z\ell}, \quad (3.3)$$

but the results teach us an important lesson which is summarized in the canonical quantum-critical phase diagram shown in Fig. 4. We ask the question: which of the relevant perturbations, s or T , is more important? To answer this question, we integrate the RG equations to a scale $\ell = \ell^*$ until the winner reaches a value of unity. This allows us to conclude that for $T > |s|^{z\nu}$, thermal effects are more important than any deviation of the coupling from the RG fixed point. Conversely, for $T < |s|^{z\nu}$ the couplings flow far from the critical fixed

point before any thermally excited states need be considered. These considerations lead to the two distinct regimes show in Fig. 4.

In the blue-colored regimes of Fig. 4, where $T < |s|^{z\nu}$, the physics of the two non-critical phases dominates. For the model of Eq. (2.27), these are the semi-metal or antiferromagnetic insulator phases, both of which have well-defined quasiparticle excitations. Consequently, the long-time dynamics can be written using quasi-classical models of the interactions of these quasiparticles.

Our interest here is primarily in the orange-colored regime of quantum criticality, $T > |s|^{z\nu}$. Here T is the primary perturbation to the quantum critical theory. The deviation of the couplings from $T = 0$ RG fixed point is unimportant, and the system behaves as it is described by the universal quantum-critical Lagrangian in the entire regime. For the relativistic model considered here, the strongly coupled CFT describes the dynamics of the orange-colored region.

It has been argued¹⁸ that a central general property of quantum critical dynamics is the short time over which the system relaxes back to thermal equilibrium. We imagine perturbing the system away from equilibrium, and measuring the time, τ_{eq} over which it relaxes back to local equilibrium (the adjective ‘local’ implies that we exclude diffusion of globally conserved charges which can take a long time to reach equilibrium across the entire system). In the regime of strongly-coupled quantum criticality this is given by

$$\tau_{\text{eq}} = \mathcal{C} \frac{\hbar}{k_B T} \quad (3.4)$$

where \mathcal{C} is a universal number dependent only upon the universality class of the transition, and precise definition used for τ_{eq} . Furthermore, in all other regimes, the value of τ_{eq} is parametrically larger than the value in Eq. (3.4). Thus quantum criticality is characterized by the *shortest possible* thermal equilibration time: this is sometimes characterized as the behavior of a *perfect fluid*.

It is important to note that our discussion above does *not* apply to CFTs in 1+1 dimensions. These are integrable systems, whose long-time dynamics is non-generic and does not generalize to higher dimensions.

A. Quantum critical transport

Let us explore the ideas above by examining the behavior of the electron conductivity of the model in Eq. (2.27) in the quantum-critical regime. At one-loop order, we can set $m = 0$, and then repeat the computation in Eq. (2.30) at $T > 0$. This only requires replacing the integral over the loop frequency by a summation over the Matsubara frequencies, which are quantized by odd multiples of πT . Such a computation, via Eq. (2.32) leads to the

conductivity¹⁹

$$\text{Re}[\sigma(\omega)] = (2T \ln 2) \delta(\omega) + \frac{1}{4} \tanh\left(\frac{|\omega|}{4T}\right); \quad (3.5)$$

the imaginary part of $\sigma(\omega)$ is the Hilbert transform of $\text{Re}[\sigma(\omega)] - 1/4$. Note that this reduces to Eq. (2.33) in the limit $\omega \gg T$. However, the most important new feature of Eq. (3.5) arises for $\omega \ll T$, where we find a delta function at zero frequency in the real part. Thus the d.c. conductivity is infinite at this order, arising from the collisionless transport of thermally excited carriers.

The relaxational processes associated with Eq. (3.4) should lead to collisions between the thermally excited carriers and broaden the delta function at zero frequency. However, this relaxation does appear in a direct perturbative analysis of the critical theory in powers of $(3-d)$ or $1/N$. As has been discussed elsewhere^{19–24}, an infinite order resummation is required, whose simplest realization requires solution of a quantum Boltzmann equation. Such a solution shows that the delta function acquires a width of order $(3-d)^2 T$ or T/N , and so there is a large d.c. conductivity of order $(3-d)^{-2}$ or N . Thus $\sigma(\omega)$ has the form of ‘Drude peak’ at zero frequency, and the behavior in Eq. (2.34) for $\omega \gg T$. However, the accuracy of such a Boltzmann equation computation is untested, and it is likely that such perturbative analyses of perfect fluid dynamics are quantitatively unreliable.

We will be satisfied here by scaling arguments which generalize the $T = 0$ quantum-critical results in Eq. (2.34) to the $T > 0$ quantum critical region in Fig. 4. The perfect fluid relaxational processes invalidate the form in Eq. (2.34) for the density correlation function, and we instead expect the form dictated by the hydrodynamic diffusion of charge. Thus for K_{00} , Eq. (2.34) applies only for $\omega \gg T$, while

$$K_{00}(\omega, k) = \chi \frac{Dk^2}{Dk^2 - i\omega} \quad , \quad \omega \ll T. \quad (3.6)$$

Here χ is the charge susceptibility (here it is the compressibility), and D is the charge diffusion constant. Associated with Eq. (3.4), these have universal values in the quantum critical region:

$$\chi = \mathcal{C}_\chi T \quad , \quad D = \frac{\mathcal{C}_D}{T}, \quad (3.7)$$

where again \mathcal{C}_χ and \mathcal{C}_D are universal numbers. For the conductivity, we expect a crossover from the collisionless critical dynamics at frequencies $\omega \gg T$, to a hydrodynamic collision-dominated form for $\omega \ll T$. This entire crossover is universal, and is described by a universal crossover function

$$\sigma(\omega) = \mathcal{K}_\sigma(\omega/T). \quad (3.8)$$

The result in Eq. (2.34) applies for $\omega \gg T$, and so

$$\mathcal{K}_\sigma(\infty) = \mathcal{K}. \quad (3.9)$$

For the hydrodynamic transport, we apply the Kubo formula in Eq. (2.32) to Eq. (3.6) and obtain

$$\mathcal{K}_\sigma(0) = \mathcal{C}_\chi \mathcal{C}_D \quad (3.10)$$

which is a version of Einstein's relation for Brownian motion.

B. The AdS/CFT correspondence

Portions of this section have been adapted from Chapter 15 of Ref. 18.

It turns out the AdS/CFT correspondence is ‘just what the doctor ordered’ to compute strongly-coupled quantum critical dynamics and transport in the orange-colored region of Fig. 4. This is a consequence of a crucial property: even at the level of the classical gravity approximation in the AdS theory, the system relaxes back to thermal equilibrium in a time which obeys Eq. (3.4). No other method in condensed matter physics shares this remarkable feature. We will review specific computations by this method of the universal function $\mathcal{K}_\sigma(\omega/T)$, and of the collisionless-to-hydrodynamic crossover in the density correlation function.

The CFT solvable by the AdS/CFT correspondence may be viewed as a generalization of the CFT described by Eq. (2.27). It has a closer resemblance to the SU(2) gauge theory we consider later in Eq. (5.8). We take the structure of critical matter fields coupled to a gauge field, and generalize it to a relativistically invariant model with a non-Abelian SU(N) gauge group and the maximal possible supersymmetry. The resulting supersymmetric Yang-Mills (SYM) theory has only one independent coupling constant g . Under the RG, it is believed that g flows to an attractive fixed point at a non-zero coupling $g = g^*$; the fixed point then defines a supersymmetric conformal field theory in 2+1 dimensions (a SCFT3). We are interested here in computing the transport properties of the SCFT, as a paradigm of quantum critical transport at a strongly interacting quantum critical point.

The solution proceeds by a dual formulation as a four-dimensional supergravity theory on a spacetime with uniform negative curvature: anti-de Sitter space, or AdS₄. The solution is also easily extended to non-zero temperatures, and allows direct computation of the correlators of conserved charges in real time. At $T > 0$ a black hole appears in the gravity theory, resulting in an AdS-Schwarzschild spacetime, and T is the Hawking temperature of the black hole; the real time solutions also extend to $T > 0$.

The reader is referred to the original paper²⁵, and to the TASI lectures by Son for an explicit description of the method. The results of a full computation of the density correlation function, $K_{00}(\omega, k)$ are shown in Fig. 5 and 6. The most important feature of these results is that the expected limiting forms in the collisionless (Eq. (2.34)) and collision-dominated (Eq. (3.6)) are obeyed. Thus the results do display the collisionless to collision-dominated crossover at a frequency of order $k_B T/\hbar$, as we expected from the physical discussion in Section III A.

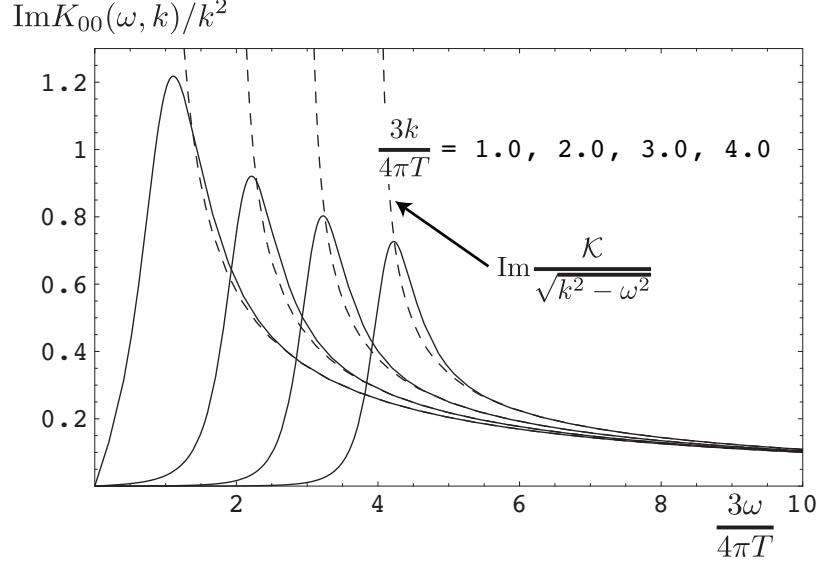


FIG. 5: Spectral weight of the density correlation function of the SCFT3 with $\mathcal{N} = 8$ supersymmetry in the collisionless regime

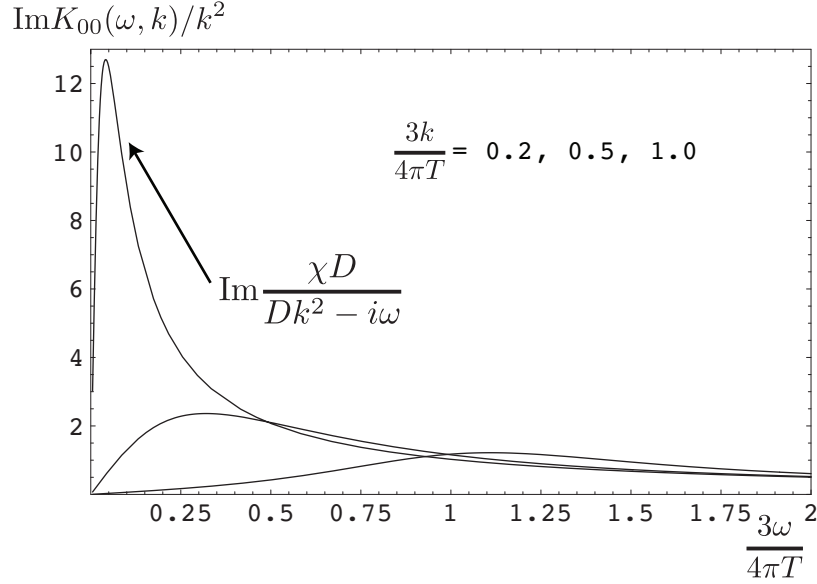


FIG. 6: As in Fig. 5, but for the collision-dominated regime.

At this point, we describe some technical aspects of the results which turn out to have important physical implications. For this, let us generalize the constraints on $K_{\mu\nu}$ from current conservation in Eq. (2.31) to non-zero temperatures. At $T > 0$, we do not expect $K_{\mu\nu}$ to be relativistically covariant, and so can only constrain it by spatial isotropy and density conservation. These two constraints, along with dimensional analyses, lead to the most general form

$$K_{\mu\nu}(\omega, k) = \sqrt{k^2 - \omega^2} \left(P_{\mu\nu}^T K^T(\omega, k) + P_{\mu\nu}^L K^L(\omega, k) \right), \quad (3.11)$$

where we are using the same symbol k to represent a 3-vector and its component 2-vector $k_\mu = (\omega, k_i)$; the interpretation should be clear from the context. $K^{L,T}$ are dimensionless functions of the arguments, and depend upon ω and the magnitude of the 2-vector k . Also $P_{\mu\nu}^T$ and $P_{\mu\nu}^L$ are orthogonal projectors defined by

$$P_{00}^T = P_{0i}^T = P_{i0}^T = 0 \quad , \quad P_{ij}^T = \delta_{ij} - \frac{k_i k_j}{k^2} \quad , \quad P_{\mu\nu}^L = \left(\eta_{\mu\nu} - \frac{p_\mu p_\nu}{p^2} \right) - P_{\mu\nu}^T, \quad (3.12)$$

with the indices i, j running over the 2 spatial components. Thus, in the general case at $T > 0$, the full density and current responses are described in terms of two functions $K^{L,T}(k, \omega)$, representing current fluctuations longitudinal and transverse to the momentum. These two functions are not entirely independent. At $T > 0$, we expect all correlations to be smooth functions at $k = 0$: this is because all correlations are expected to decay exponentially to zero as a function of spatial separation. However, this is only possible from (3.11) if we have the additional relation

$$K^T(\omega, 0) = K^L(\omega, 0). \quad (3.13)$$

The relations of the previous paragraph are completely general and apply to any theory. Specializing to the AdS-Schwarzschild solution of SYM3, the results were found to obey a simple and remarkable identity²⁵:

$$K^L(\omega, k) K^T(\omega, k) = \mathcal{K}^2 \quad (3.14)$$

where \mathcal{K} is a known pure number, independent of ω and k . Let us give some more details on the origin of (3.14). In the AdS/CFT correspondence, every globally conserved quantity in the CFT gets mapped onto a gauge field in AdS. Moreover, in the leading classical gravity theory on AdS, different global charges commute with each other, and so can be considered separately. In the end, we have a U(1) gauge field on AdS for every global conservation law of the CFT. The low energy effective field theory on AdS₄ has the standard Einstein-Maxwell action for gravity+electromagnetism. The Maxwell action is in 3+1 dimensions, and this is well-known to have a self-dual structure corresponding to the exchange of electric and magnetic fields. Thus we have the important and key result that every global charge in a CFT3 maps onto a self-dual theory in the leading gravity approximation on AdS₄. The identity in (3.14) is a consequence of this emergent self-duality of CFT3s.

The combination of (3.14) and (3.13) now fully determine the response functions at zero momenta: $K^L(\omega, 0) = K^T(\omega, 0) = \mathcal{K}$. Computing the conductivity from Eq. (2.32), we then have

$$\sigma(\omega) = \mathcal{K}_\sigma(\omega/T) = \mathcal{K}; \quad (3.15)$$

i.e. the scaling function in Eq. (3.8) is independent of ω and equal to the value in Eq. (3.9).

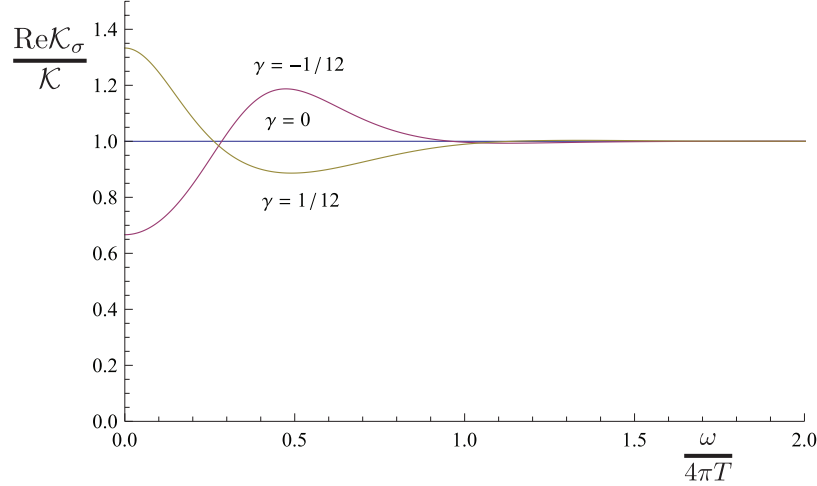


FIG. 7: Frequency dependent conductivity for CFT3s for which the AdS_4 theory includes the leading correction beyond the Einstein-Maxwell theory²⁶. The co-efficient of this correction is γ , and stability requirements impose the bound $|\gamma| < 1/12$.

This result is an important surprise: the conductivity of the classical gravity theory on AdS_4 is frequency-independent. Furthermore, its value is fixed by self-duality to be the constant \mathcal{K} appearing in the self-duality relation (3.14). All these remarkable results are a direct consequence of the self-duality of the $\text{U}(1)$ Maxwell theory on AdS_4 .

Given the strong consequences of self-duality relation in Eq. (3.14), it is useful to ask whether it can be valid for CFTs beyond those described by the classical Einstein-Maxwell theory on AdS_4 . This question was addressed recently by Myers *et al.*²⁶. They examined the leading corrections beyond the Einstein-Maxwell theory in an effective theory of AdS_4 , and found that a generalized duality relation applied also to this theory. However, this duality was not a *self*-duality, and so we considerably less restrictive. The dual CFT had current correlation functions which were characterized by functions $\tilde{K}^{L,T}(\omega, k)$ which were distinct from those of the direct CFT $K^{L,T}(\omega, k)$, and the self-duality relation of Eq. (3.14) took the less restrictive form

$$K^L(\omega, k) \tilde{K}^T(\omega, k) = \mathcal{K}^2 \quad , \quad K^T(\omega, k) \tilde{K}^L(\omega, k) = \mathcal{K}^2. \quad (3.16)$$

These duality relation determines the correlators of the dual CFT in terms of the direct CFT, but do not fix the latter. Determine of the functions $K^L(\omega, 0) = K^T(\omega, 0)$ requires explicit computation on the extended theory on AdS_4 , and the results for the conductivity are presented in Fig. 7. Now the conductivity does have a non-trivial universal dependence on ω/T . However, as is clear from Fig. 7, stability conditions on the effective theory on AdS_4 allow only a limited range of dependence on ω/T . The smooth ω/T dependence in Fig. 7 should be contrasted to the very singular dependence in the free-field result in Eq. (3.5); the former is clearly more generic for a strongly-coupled CFT. It is also interesting to note

that the ω/T dependence in Fig. 7 for $\gamma > 0$ is very similar to the structure we discussed in Section III A on the effect of collisional broadening of the singularities in Eq. (3.5): the AdS_4 result shows a collision-dominated Drude peak at $\omega = 0$, and a collisionless critical continuum at large ω .

Does the duality mapping of Myers *et al.*²⁶ have an interpretation directly in the CFT, without using the mapping to AdS_4 ? It has been argued^{25–27} that this duality is the analog of the ‘particle-vortex’ duality of condensed matter physics. The latter is an exact duality of the critical theory of a complex relativistic scalar field²⁸ (this the theory in Eq. (2.27) without the fermions, and with φ^a having two components). In the particle-vortex duality, the world line of the complex scalars is reinterpreted as the world line of vortices in the dual theory of a dual complex scalar interacting with an emergent electromagnetic field.

Let us summarize the lessons we have learnt from the AdS theory of quantum critical transport in strongly interacting systems in 2+1 dimensions. This theory should be viewed as complementary to the quasiparticle-based theory, whose implications were discussed in Section III A. The lessons are:

- There are a large class of strongly interacting 2+1 dimensional quantum ‘perfect fluids’ which are able to relax back to thermal equilibrium in a time of order $\hbar/(k_B T)$, as we indicated in (3.4).
- A good first approximation for a transport theory of such perfect fluids is the classical Einstein-Maxwell theory on AdS_4 .
- The Einstein-Maxwell theory exhibits collisionless dynamics for $\omega \gg T$, and collision-dominated dynamics for $\omega \ll T$, as we displayed in Figs. 5 and 6.
- All continuous global symmetries are represented by a self-dual Einstein-Maxwell theory.
- This emergent self-duality implies that $\sigma(\omega)$ is frequency-independent in the Einstein-Maxwell theory and equal to the self-dual value.
- A frequency dependent conductivity is obtained²⁶ upon considering corrections to the effective Einstein-Maxwell theory, with the form in Fig. 7. Stability conditions on the effective theory strongly restrict the range of frequency dependence.
- Such quantum perfect fluids also have universal momentum transport. By extending the scaling arguments to momentum transport we would conclude that the ratio of the shear viscosity to the entropy density η/s should equal a universal number characterizing the collision-dominated regime. This number was computed in the Einstein-Maxwell theory by Kovtun *et al.*^{29,30} and found to equal $\hbar/(4\pi k_B)$.

IV. U(1) GAUGE THEORY AND THE VALENCE BOND SOLID ON THE HONEYCOMB LATTICE

We now return to the honeycomb lattice at half-filling. In Section IID we described a quantum phase transition in which two characteristics of the ground state changed simultaneously. In the charge sector, the one electron excitation gap opened up leading to a transition from the semi-metal to the insulator. And in the spin sector, the breaking of SU(2) spin rotation symmetry led to Néel order in the insulator. However, in the Mott picture, the insulating behavior is tied to repulsion between the electrons, which keeps them apart, rather than to any specific symmetry breaking. This would suggest that it is possible to have an insulating state while preserving spin rotation invariance. We will explore such a possibility in the present section.

Our approach will be begin in the Néel-ordered insulator, and restore spin rotation invariance by allowing for slow angular fluctuations in the local *orientation* of the Néel order parameter φ^a . At the same time, it will also pay to transform the fermions to a ‘rotating reference frame’ so that their spin is measured relative to the orientation of the local Néel order^{31–33}. This transformation is most conveniently done using spinor variables. So let us decompose the vector Néel order φ^a into a complex two-component bosonic spinor z_α by

$$\varphi^a = z_\alpha^* \sigma_{\alpha\beta}^a z_\beta \quad (4.1)$$

Such a decomposition is familiar from early work of D’Adda *et al.*³⁴ and Witten³⁵, who established the equivalence between the O(3) non-linear σ -model and the CP¹ model in 2 spacetime dimensions. A similar equivalence does not immediately apply in the 3 spacetime dimensional case of interest here because point defects in spacetime have to be treated with some care³⁶. In particular, the theory for the fluctuations of the vector field φ^a must allow for point spacetime defects (‘instantons’) where $\varphi^a = 0$, which are known in the condensed matter literature as ‘hedgehogs’. Note that these hedgehogs are present even in a ‘fixed-length’, non-linear σ -model in which we set $\varphi^{a2} = 1$; such models require ultraviolet regularization, and the hedgehogs are invariably permitted in the regulated theory *e.g.* with a lattice regularization. Ignoring these defects momentarily, let us proceed as in the earlier work^{34,35}. The parameterization in Eq. (4.1) is invariant under the U(1) gauge transformation

$$z_\alpha \rightarrow z_\alpha e^{i\zeta} \quad (4.2)$$

and so the theory for the z_α must be a U(1) gauge theory involving an emergent U(1) gauge field A_μ . The boson only terms in Eq. (2.27) are equivalent^{34,35} to a U(1) gauge theory for the complex scalars z_α

$$\mathcal{L}_z = |(\partial_\mu - iA_\mu)z_\alpha|^2 + s|z_\alpha|^2 + u(|z_\alpha|^2)^2. \quad (4.3)$$

Here the gauge field A_μ is dynamical, and will acquire a Maxwell action after high energy z_α modes have been integrated out.

Let us now discuss the point defects. Eqn (4.1) implies³⁶ that the hedgehogs in φ^a become Dirac monopoles in A_μ : these are tunnelling events associated with a change in the total A_μ flux by 2π . Such monopoles are permitted by the U(1) gauge theory in Eq. (4.3) only if the U(1) gauge field is *compact*. So we must account for the dynamics of such a compact U(1) gauge theory to completely account for the fluctuations of the local antiferromagnetic order. The dynamics of the matter fields can suppress the monopoles in some cases^{37–39}, and this can then lead to deconfined critical points or phases with a gapless U(1) photon excitation associated with an effectively non-compact U(1) gauge field. We will find an example of this phenomenon in Section VI.

Let us now turn to the fermionic excitations in antiferromagnetic insulator. We transform these to the rotating reference frame by writing^{31–33}

$$\begin{pmatrix} c_\uparrow \\ c_\downarrow \end{pmatrix} = \begin{pmatrix} z_\uparrow & -z_\downarrow^* \\ z_\downarrow & z_\uparrow^* \end{pmatrix} \begin{pmatrix} \psi_+ \\ \psi_- \end{pmatrix} \quad (4.4)$$

where ψ_p , $p = \pm$, are the “electrons” in the rotating reference frame. The index p measures the spin-projection along the direction of the local Néel order. However, more properly it is the “charge” under the emergent U(1) gauge field because Eq. (4.4) is invariant under Eq. (4.2) and

$$\psi_+ \rightarrow \psi_+ e^{-i\zeta} \quad , \quad \psi_- \rightarrow \psi_- e^{i\zeta}. \quad (4.5)$$

An important consequence of Eqs. (4.4) and (4.1) is the identity

$$\varphi^a c_\alpha^\dagger \sigma_{\alpha\beta}^a c_\beta = (|z_\alpha|^2)^2 \left(\psi_+^\dagger \psi_+ - \psi_-^\dagger \psi_- \right). \quad (4.6)$$

Thus the effective moment acting on the ψ fermions is always along the z axis, as expected by the transformation to a rotating reference frame.

Let us now take the continuum limit for the fermions in the rotating reference frame. We follow exactly the same mapping as in Eq. (2.8) to map the lattice ψ fermions to continuum 8-component Ψ fermions. Based upon Eq. (4.6), we also expect the Ψ fermions to experience a field polarized along the σ^z direction. Combined with gauge invariance, and the structure of Eq. (2.27), we are led to the following Lagrangian density for Ψ :

$$\mathcal{L}_\Psi = \bar{\Psi} \gamma_\mu (\partial_\mu + i\sigma^z A_\mu) \Psi - \lambda N_0 \bar{\Psi} \rho^z \sigma^z \Psi. \quad (4.7)$$

Note this is the theory of Dirac fermions of mass $|\lambda N_0|$ coupled to a U(1) gauge field.

The Lagrangian $\mathcal{L}_z + \mathcal{L}_\Psi$ is then our U(1) gauge theory for the fluctuating Néel state, complementary to the Gross-Neveu-Yukawa theory in Eq. (2.27). The remainder of this section is devoted to understanding the physical properties of $\mathcal{L}_z + \mathcal{L}_\Psi$.

Let us now discuss the phases of this U(1) gauge theory.

First, we have the Higgs phase, where $s < 0$ and z_α is condensed. Here the U(1) photon is gapped, and spin rotation invariance is broken. This is just the insulating Néel state, and its properties are identical to the Néel ordered state described by Eq. (2.27).

The other phase with $s > 0$ has z_α gapped and spin rotation invariance is preserved. However, as is clear from Eq. (4.7), the fermionic spectrum remains gapped. Thus this phase is clearly not the semi-metal of Eq. (2.27). Instead it is a new insulating phase with spin rotation invariance preserved. Thus we have achieved our objective of describing an insulator without Néel order.

However, this insulator is not a featureless state with a spin and a charge gap, as we will now show. The interesting physics arises from an interplay of the monopole events with the filled band of fermionic states. If we integrate out this filled band via \mathcal{L}_Ψ , we generate an effective Maxwell action for the U(1) gauge field

$$\mathcal{L}_A = \frac{1}{12\pi|\lambda N_0|}(\epsilon_{\mu\nu\lambda}\partial_\nu A_\lambda)^2 \quad (4.8)$$

We recall that the U(1) gauge field is compact, and it was shown by Polyakov⁴⁰ that such a gauge field always acquires a mass gap and is in a confining phase in 2+1 dimensions. The confinement is caused by the proliferation of monopole tunneling events. Here we will show^{12,36,39,41} that the monopole operator has non-trivial transformation properties under the symmetry group of the honeycomb lattice: consequently, the proliferation of monopoles in the confining phase breaks a lattice symmetry due to the appearance of valence bond solid (VBS) order.

To see this, it is useful to add an external source B_μ to the fermion Lagrangian in Eq. (4.7) so that \mathcal{L}_Ψ becomes

$$\mathcal{L}_\Psi = \bar{\Psi}\gamma_\mu(\partial_\mu + i\sigma^z A_\mu)\Psi - \lambda N_0 \bar{\Psi}\rho^z\sigma^z\Psi - \frac{i}{2}B_\mu\bar{\Psi}\gamma_\mu\rho^z\Psi. \quad (4.9)$$

This source has been judiciously chosen so that when we integrate out the fermions, the action for the A_μ gauge field in Eq. (4.8) acquires a mutual Chern-Simons term^{12,41}

$$\mathcal{L}_A = \frac{1}{12\pi|\lambda N_0|}(\epsilon_{\mu\nu\lambda}\partial_\nu A_\lambda)^2 + \frac{i}{2\pi}B_\mu\epsilon_{\mu\nu\lambda}\partial_\nu A_\lambda \quad (4.10)$$

Let us now proceed with Polyakov's duality mapping on Eq. (4.10) to obtain an effective theory of monopoles: the B_μ source term will allow us to deduce the connection between the monopole operator and the underlying lattice fermions. The first step corresponds to decoupling the Maxwell term by a Hubbard-Stratonovich field, Y_μ , to obtain

$$\mathcal{L}_A = \frac{3|\lambda N_0|}{4\pi}Y_\mu^2 + \frac{i}{2\pi}Y_\mu\epsilon_{\mu\nu\lambda}\partial_\nu A_\lambda + \frac{i}{2\pi}B_\mu\epsilon_{\mu\nu\lambda}\partial_\nu A_\lambda \quad (4.11)$$

Now, we integrate over A_μ , and this yields the constraint

$$Y_\mu = \partial_\mu \phi - B_\mu. \quad (4.12)$$

where ϕ is the scalar field which is dual to the photon. We have judiciously chosen factors of (2π) above to ensure a normalization so that $e^{i\phi}$ is the monopole operator. Finally, inserting Eq. (4.12) into (4.11) we obtain^{12,41}

$$\mathcal{L}_\phi = \frac{3|\lambda N_0|}{4\pi} (\partial_\mu \phi - B_\mu)^2. \quad (4.13)$$

In the absence of the external source B_μ , this free scalar field theory implies that the monopole operator $e^{i\phi}$ has long-range correlations in 2+1 dimensions.

The B_μ term in Eq. (4.13) will help us link the monopole operator to the underlying electrons⁴¹. First, we notice that the theory in Eq. (4.9) actually enjoys a gauge invariance under which

$$\Psi \rightarrow \exp\left(i\frac{\rho^z}{2}\theta\right)\Psi \quad , \quad B_\mu \rightarrow B_\mu - \partial_\mu \theta \quad (4.14)$$

where θ is a field with an arbitrary spacetime dependence. (Note that this gauge invariance is distinct from that associated with the A_μ gauge field in Eq. (4.5), under which $\Psi \rightarrow \exp(-i\sigma^z\zeta)\Psi$.) Now we observe that this gauge invariance extends also to Eq. (4.13), under which

$$e^{i\phi} \rightarrow e^{i\theta} e^{i\phi}. \quad (4.15)$$

The combination of Eqs. (4.14) and (4.15) now allows us to identify the operator $e^{i\phi}$. We look for a fermion bilinear of the form $\bar{\Psi}M\Psi$ so it transforms like Eq. (4.15) under the gauge transformation in Eq. (4.14). Moreover, the Lorentz invariance of the theory implies that the matrix M should commute with the γ_μ matrices in Eq. (2.12). This leads us to the unique choice

$$e^{i\phi} \sim \bar{\Psi}\tau^y(\rho^x + i\rho^y)\Psi \sim \bar{C}\tau^y(\rho^x + i\rho^y)C \quad (4.16)$$

It now remains to use the geometric definitions in Section II A and Eq. (2.8) to deduce the physical interpretation of the fermion bilinear in Eq. (4.16). A careful analysis⁴¹ along these lines shows that $e^{i\phi}$ is an operator associated with the valence bond solid (VBS) order in Fig. 8.

Thus we reach our main conclusion: the insulating phase without Néel order as described by the U(1) gauge theory $\mathcal{L}_z + \mathcal{L}_\Psi$ has long-range VBS order. This order onsets with the confinement induced by the proliferation of monopoles.

It is interesting to note that the matrices in the fermion bilinears associated with VBS order $\sim \bar{C}\tau^y(\rho^x + i\rho^y)C$ and Néel order $\sim \bar{C}\rho^z\sigma^a C$ all anti-commute with each other, and commute with the γ_μ matrices in Eq. (2.12). This can be used to formulate the present

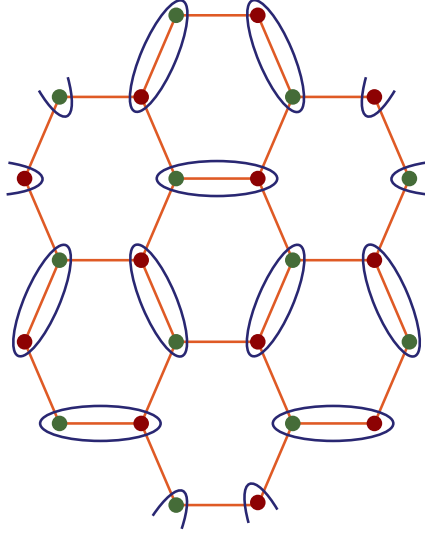


FIG. 8: A schematic illustration of the valence bond solid (VBS). The ellipses represent singlet valence bonds between the electrons. These reside preferentially in the pattern shown in the VBS state. Expectation values of all spin-singlet observables, such as $S_i^a S_j^a$ or $c_{i\alpha}^\dagger c_{j\alpha} + c_{j\alpha}^\dagger c_{i\alpha}$, are different on the links with the ellipses than those without.

theory without gauge fields but using a Wess-Zumino-Witten term^{41–45}: we will not explore this approach here.

We can also use the methods of this section to address the nature of the transition between the Néel and VBS phases. We will not go into details here, but this transition has been proposed^{38,39} to be a deconfined critical point at which monopoles are suppressed, and the critical theory is the non-compact version of the U(1) gauge theory given by \mathcal{L}_z .

V. SU(2) GAUGE THEORY AND A PHASE DIAGRAM FOR THE HALF-FILLED HONEYCOMB LATTICE

Sections II and IV have so far described 3 possible phases of the honeycomb lattice at half-filling: the semi-metal, the insulator with Néel order, and the insulator with VBS order. The first two phases appear in the theory \mathcal{L} in Eq. (2.27), while the latter two appear in the theory $\mathcal{L}_z + \mathcal{L}_\Psi$ in Eqs. (4.3) and (4.7). This is an unsatisfactory state of affairs: we would like to write down a single unified theory in which all 3 phases appear. One approach, implicitly mentioned above, is to extend Eq. (2.27) by including an additional two-component real scalar field representing the VBS order parameter, and couple it to the fermion bilinear $\bar{C}\tau^y(\rho^x + i\rho^y)C$ appearing in Eq. (4.16). Integrating out the fermions in the background of a spatially varying 5-component scalar representing the Néel and VBS orders yields a Wess-Zumino-Witten term for the scalar field^{41–45}. The resulting theory is difficult to work with, and little is known about it in the regime where all three phases can meet.

Here we will present an alternative approach which allows for exotic phases using an

emergent SU(2) gauge field. We will find that the resulting phase diagram has a fourth semi-metallic phase with an emergent topological order, and an interesting multicritical point.

Our starting point is the observation that the decomposition of the electron into spinful bosons and spinless charged fermions in Eq. (4.4) has a larger gauge invariance³³ than U(1). Rewriting eq. (4.4) using a natural matrix notation

$$c = R\psi \quad (5.1)$$

where

$$R \equiv \begin{pmatrix} z_{\uparrow} & -z_{\downarrow}^* \\ z_{\downarrow} & z_{\uparrow}^* \end{pmatrix}, \quad (5.2)$$

we note that Eq. (5.1) is invariant under the gauge transformation generated by SU(2)_g matrix U under which

$$R \rightarrow RU^\dagger, \quad \psi \rightarrow U\psi, \quad c \rightarrow c. \quad (5.3)$$

This SU(2)_g gauge transformation should be distinguished from the global SU(2) spin rotation V , under which

$$R \rightarrow VR, \quad \psi \rightarrow \psi, \quad c \rightarrow Vc. \quad (5.4)$$

Turning to the Néel order φ^a , this clearly transforms as a **3** under the global SU(2). However, the parameterization for the Néel order in Eq. (4.1) is not invariant the SU(2)_g gauge transformation in Eq. (5.3). As written, Eq. (4.1) is invariant only under the U(1) gauge transformation in Eq. (4.2) which was the reason for our original choice of a U(1) gauge theory in Section IV. Thus we cannot use Eq. (4.1) as our definition of the Néel order in the present SU(2) gauge theory.

It is more natural to proceed here^{12,33} by defining the scalar fields using bilinears of the fermions. Thus using Eq. (2.25) and extending to continuum 8-component fermions near the Fermi points, we define

$$\varphi^a = \bar{C}\rho^z\sigma^a C. \quad (5.5)$$

From this definition it is clear that φ^a transforms as a **3** under the global SU(2), while it is invariant under SU(2)_g, just as expected.

We can also define the corresponding scalar using the ψ fermions³³:

$$\Phi^a = \bar{\Psi}\rho^z\sigma^a\Psi. \quad (5.6)$$

Now Φ^a transforms as a **3** under the gauge SU(2)_g, while it is invariant under SU(2).

From Eqs. (5.1), (5.5) and (5.6), we find that the scalar fields are related by

$$\begin{aligned}\varphi^a &= \frac{1}{2}\Phi^b \text{Tr}(\sigma^a R \sigma^b R^\dagger) \\ \Phi^a &= \frac{1}{2}\varphi^b \text{Tr}(\sigma^b R \sigma^a R^\dagger) (|z_\alpha|^2)^2.\end{aligned}\tag{5.7}$$

These relations generalize Eq. (4.1) from the U(1) gauge theory.

To summarize, the matter fields of our $\text{SU}(2)_g$ gauge theory are the bosonic matrix R , the fermions Ψ , and the scalar Φ^a . As in Section IV, we will also need an emergent dynamic $\text{SU}(2)_g$ gauge field A_μ^a . Using symmetry and gauge invariance, we can now write down the following Lagrangian density³³ for the SU_g gauge theory; this combines and generalizes the Gross-Neveu-Yukawa model in Eq. (2.27), and U(1) gauge theory in Eqs. (4.3) and (4.7).

$$\begin{aligned}\mathcal{L}_g &= \bar{\Psi}\gamma_\mu(\partial_\mu + i\sigma^a A_\mu^a)\Psi - \lambda\Phi^a\bar{\Psi}\rho^z\sigma^a\Psi \\ &+ \frac{1}{2}\left[(\partial_\mu\Phi^a - 2\epsilon_{abc}A_\mu^b\Phi^c)^2 + s\Phi^{a2}\right] + \frac{u}{24}(\Phi^{a2})^2 \\ &+ \text{Tr}\left[(\partial_\mu R - iA_\mu^a R\sigma^a)(\partial_\mu R^\dagger + iA_\mu^a \sigma^a R^\dagger)\right] \\ &+ \tilde{s}\text{Tr}(RR^\dagger) + \tilde{u}\left[\text{Tr}(RR^\dagger)\right]^2.\end{aligned}\tag{5.8}$$

This Lagrangian combines all three phases discussed so far, and forms the basis of our remaining discussion of the honeycomb lattice at half-filling.

In mean-field theory, the model \mathcal{L}_g has 4 phases, depending upon whether one or both of the scalar fields Φ^a and R are condensed. These 4 phases can be identified using the methods developed in Section II D and IV, and lead to the phase diagram shown in Fig. 9. First, we describe how \mathcal{L}_g reproduces the phases and phase transitions already discussed:

- The Higgs phase where $\langle R \rangle \neq 0$ breaks $\text{SU}(2)_g$ completely. Using $\text{SU}(2)_g$ gauge invariance we may as well set $R = 1$. Then from Eq. (5.7), we have $\Phi^a \sim \varphi^a$, the Néel order parameter. Also the gauge boson A_μ^a is gapped and can be neglected. Then the theory \mathcal{L}_g reduces to the Gross-Neveu-Yukawa model in Eq. (2.27). As discussed in Section II D, this theory has semi-metal and insulating Néel phases, and these are shown in Fig. 9.
- The Higgs phase where $\langle N^a \rangle \neq 0$ breaks $\text{SU}(2)_g$ down to U(1). Then only the A_μ^z (say) gauge boson is active, and the theory \mathcal{L}_g reduces to the U(1) gauge theory $\mathcal{L}_z + \mathcal{L}_\Psi$ discussed in Section IV. The insulating Néel and insulating VBS phases found there are also shown in Fig. 9.

The possible new phase of \mathcal{L}_g is the deconfined phase where both Φ^a and R are gapped. Then the low energy theory of \mathcal{L}_g is simply massless QCD with the Lagrangian density

$$\mathcal{L}_{QCD} = \bar{\Psi}\gamma_\mu(\partial_\mu + i\sigma^a A_\mu^a)\Psi.\tag{5.9}$$

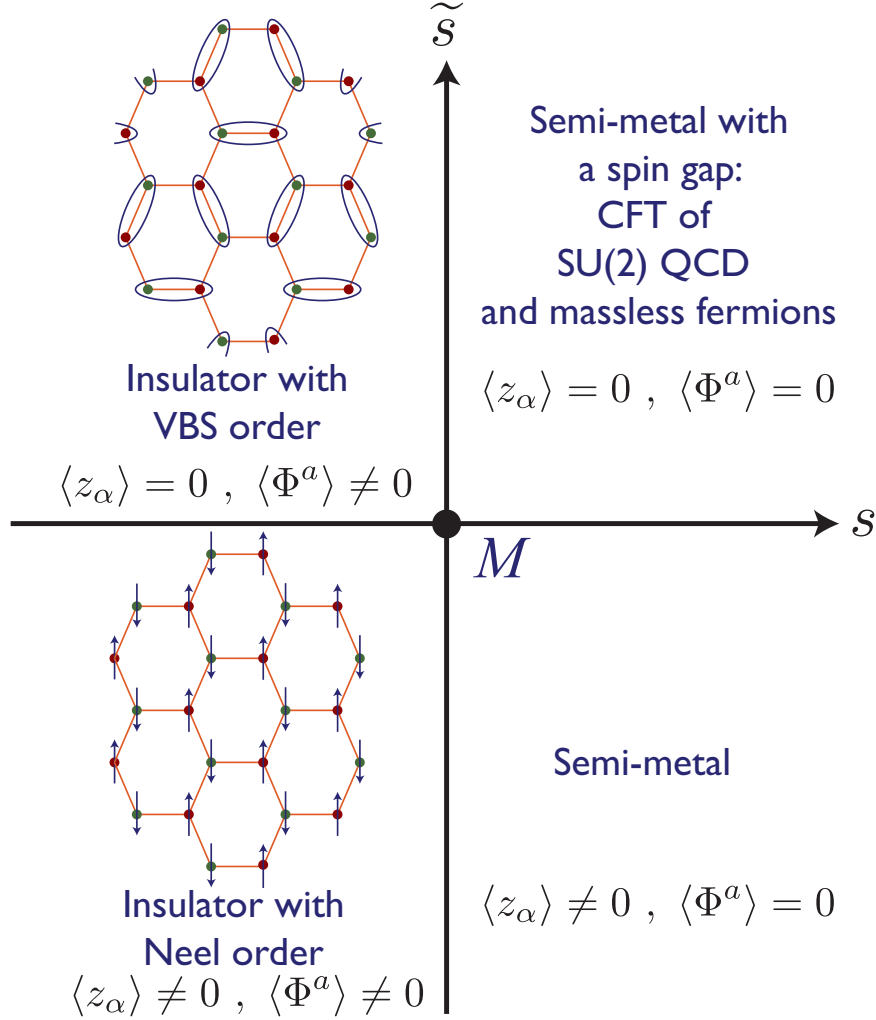


FIG. 9: Schematic phase diagram of the $SU(2)_g$ gauge theory \mathcal{L}_g in Eq. (5.4). The two phases in the bottom are described by the Gross-Neveu-Yukawa model in Eq. (2.27), while the two phases on the left are described by the $U(1)$ gauge theory $\mathcal{L}_z + \mathcal{L}_\Psi$ in Eqs. (4.3) and (4.7).

This QCD with a $SU(2)_g$ gauge group with massless 2-component Dirac fermions which carry $N_c = 2$ colors and $N_f = 2$ flavors. When N_f is large enough, it can be shown from a $1/N_f$ expansion that the confining tendencies of non-Abelian gauge fields are screened, and \mathcal{L}_{QCD} describes a non-trivial CFT, with anomalous dimensions for all observables which are not currents of global flavor or spacetime symmetries. It is an open question whether such a critical phase is allowed for $N_f = 2$, as we have assumed in Fig. 9. If not, then this phase will be unstable to confinement into one of the other phases of Fig. 9. If present, this deconfined phase would be a topologically ordered semi-metal with a spin gap; it is an ‘algebraic charge liquid’ (ACL) in the notation of Ref. 46. The gapless Ψ fermions carry electromagnetic charge, and so there is no gap to charged excitations and this phase is not an insulator. However, the Ψ fermions are spinless, and $SU(2)$ spin is only carried by the gapped bosonic excitations; hence the spin gap.

Fig 9 also shows an interesting multi-critical point M , where all 4 phases meet; if the massless QCD phase is confining, this would be the meeting point of 3 phases. Here the $SU(2)_g$ gauge bosons, the scalars Φ^a and R , and the fermions Ψ are all gapless and critical. Thus M realizes a non-trivial CFT which can be perturbed by the two relevant directions of the plane of Fig. 9. Indeed, it is not unreasonable to view this multicritical M theory as a non-supersymmetric analog of the M-theory of strings!

VI. FERMION LIQUIDS AND FRACTIONALIZED FERMION LIQUIDS

This last section briefly discusses the physically most important case: metallic systems with Fermi surfaces.

Here, the most common phase is the Fermi liquid (FL). This is the state adiabatically connected to the metallic state of non-interacting electrons. It has long-lived fermionic quasiparticle excitations along the Fermi surface, and the area enclosed by this Fermi surface obeys the Luttinger theorem which we will review shortly below.

We wish to explore other compressible phases of strongly interacting electrons at generic densities which do not break any global symmetries. There are only a few theoretical proposals for such a state, and we shall focus here on the one^{2,3} known as the fractionalized Fermi liquid (FL*). In principle, the FL* state can appear in a variety of models of correlated electrons, including ones with a single band, and all the sites equivalent with $U_i = U$. Such single-band FL* states have been described in recent work^{46–52}. However, these single-band analyses are involved, and require intermediate steps which make them sub-optimal for a first description of the FL* state.

Instead, we will introduce the FL* state in a model with 2 types of inequivalent sites. As a simple example, consider the Hubbard model on a bilayer triangular lattice shown in Fig. 10. We label the two layers as a and b , and so there are 2 electron operators, $c_{ai\alpha}$ and $c_{bi\alpha}$. We write the Hamiltonian as

$$\begin{aligned}
H &= H_a + H_b + H_{ab} \\
H_a &= -t_a \sum_{\langle ij \rangle} c_{ai\alpha}^\dagger c_{aj\alpha} + \text{H.c.} + (\epsilon_a - \mu) \sum_i (n_{ai\uparrow} + n_{ai\downarrow}) \\
&\quad + U_a \sum_i \left(n_{ai\uparrow} - \frac{1}{2} \right) \left(n_{ai\downarrow} - \frac{1}{2} \right) \\
H_b &= -t_b \sum_{\langle ij \rangle} c_{bi\alpha}^\dagger c_{bj\alpha} + \text{H.c.} + (\epsilon_b - \mu) \sum_i (n_{bi\uparrow} + n_{bi\downarrow}) \\
&\quad + U_b \sum_i \left(n_{bi\uparrow} - \frac{1}{2} \right) \left(n_{bi\downarrow} - \frac{1}{2} \right) \\
H_{ab} &= -w \sum_i c_{ai\alpha}^\dagger c_{bi\alpha} + \text{H.c.}
\end{aligned} \tag{6.1}$$

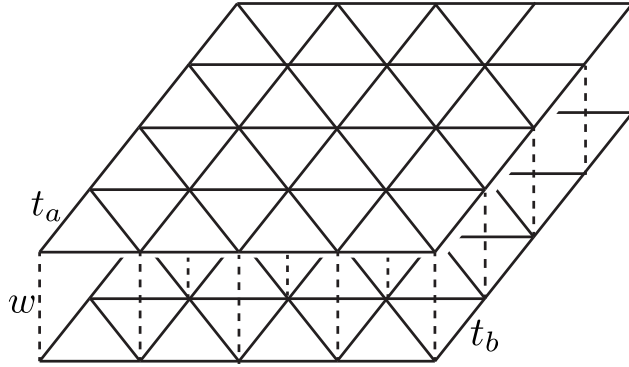


FIG. 10: The bilayer triangular lattice. The top layer (a) has nearest neighbor hopping t_a , the bottom layer (b) and nearest neighbor hopping t_b , and the inter-layer hopping is w . A closely related model is realized in the experiments of Ref. 5.

Here the sites i, j lie on a triangular lattice, and $\langle ij \rangle$ represents the sum over nearest-neighbor pairs. The Hubbard models on the two layers have distinct values of the hopping parameters, on-site repulsion, and on-site energies $\epsilon_{a,b}$. Finally, there is an on-site interlayer tunneling, w . Experiments⁵ on bilayer films of ^3He adsorbed on graphite provide a remarkable realization of a closely related model.

First, let us discuss the FL state, where $U_{a,b}$ can be treated perturbatively. Diagonalizing the one-electron Hamiltonian, we find two bands corresponding to the bonding and anti-bonding states between the two layers. Let \mathcal{N} be the total density of electrons for each bilayer site of the triangular lattice. So

$$\sum_{\alpha} \left(\langle c_{a\alpha}^{\dagger} c_{a\alpha} \rangle + \langle c_{b\alpha}^{\dagger} c_{b\alpha} \rangle \right) = \mathcal{N}. \quad (6.2)$$

This relation holds for every site i , and the site-index has been left implicit. Depending upon the value of \mathcal{N} and interlayer tunneling w , one or both of the bands will be occupied, leading to one or two Fermi surfaces. Let the areas enclosed by the Fermi surfaces be \mathcal{A}_1 and \mathcal{A}_2 ; if there is only one Fermi surface, $\mathcal{A}_2 = 0$. Luttinger's theorem fixes the areas of Fermi surfaces to a value which is independent of the nature of the electron-electron interactions. There is one Luttinger theorem for each global U(1) symmetry of the Hamiltonian which is not spontaneously broken in the ground state⁵³. Here, the total numbers of both up-spin and down-spin electrons are separately conserved, and so there are 2 Luttinger constraints. However, we will implicitly only consider states in which spin rotation invariance is preserved, and so there is only a single constraint. The constraint is the same as that for non-interacting electrons, which is

$$\frac{\mathcal{A}_1 + \mathcal{A}_2}{2\pi^2} = \mathcal{N}. \quad (6.3)$$

We will implicitly assume $\mathcal{N} > 1$ below.

We now wish to induce a quantum phase transition to FL* state. This is most easily done in a model in which the electron correlations in one layer (say a) are stronger than in the other. This can be achieved by *e.g.* choosing $U_a \gg U_b$; then for suitable choices of $\epsilon_a - \epsilon_b$, electronic states with exactly one electron on each site on layer a will be preferred, as the on-site repulsion will send all states with 0 or 2 electrons on any layer a site to high energy. Actually, we could even have $U_a = U_b$, as long as the density of electrons on layer a is close to unity, while that on layer b is small: then the dilute gas on layer b can be treated perturbatively in the two-particle scattering amplitude, while layer a will require the analog of the strong correlation methods of Section IV. It is customary at this point to follow the analysis of Section II C, and project onto this restricted Hilbert space, while using a canonical transformation to derive an effective Hamiltonian. The restricted space has only spin degrees of freedom on a lattice sites, and as in Section II C, these spins have exchange interactions with each other. The canonical transformation also generates exchange interactions between electrons separate layers, and this is known as the Kondo exchange interaction. The resulting Hamiltonian is the Kondo-Heisenberg model. However, we will not take this step here, and continue to work with the Hubbard model in Eq. (6.1).

We wish to induce a spin liquid state on layer a . In the absence of the coupling w to layer b , this state would be an insulator which preserved spin rotation invariance. However, as we will see below, the deconfined excitations in such a state can survive when w is non-zero and the ground state is a FL* metal. We will take a simple model for this spin liquid state: one with an emergent U(1) gauge boson and neutral, spinful fermionic excitations along a Fermi surface^{54,55}. This spin liquid is an ‘algebraic spin liquid’ (ASL), in the notation of Ref. 56.

We proceed with a method which parallels that in Section IV, of transforming to a ‘rotating reference frame’. However, instead of using the frame of reference of local anti-ferromagnetic order, we use a quantum rotor to keep track of the charge on each a lattice site. Each rotor has a periodic angular co-ordinate ϑ_i with period 2π ; hence the states of the rotors are $e^{in_{ri}\vartheta_i}$ where n_{ri} is a rotor angular momentum, which takes all positive and negative integer values. We will use the state with all $n_{ri} = 0$ to represent the states with one electron each a lattice site. The analog of the transformation to a rotating reference frame in Eq. (4.4) is now⁵⁷

$$c_{a\alpha} = e^{-i\vartheta} f_{\alpha} \quad (6.4)$$

where we have dropped the implicit site index, and f_{α} are neutral fermions (‘spinons’) which keep track of the orientation of the electron. We can now identify the 4 states on each a lattice site in Eq. (2.13) with corresponding states of the rotor and spinons:

$$\begin{aligned} |0\rangle &\Leftrightarrow e^{-i\vartheta}|0\rangle \\ c_{\alpha}^{\dagger}|0\rangle &\Leftrightarrow f_{\alpha}^{\dagger}|0\rangle \\ c_{\uparrow}^{\dagger}c_{\downarrow}^{\dagger}|0\rangle &\Leftrightarrow e^{i\vartheta}f_{\uparrow}^{\dagger}f_{\downarrow}^{\dagger}|0\rangle \end{aligned} \quad (6.5)$$

Note that these allowed states obey the constraint

$$f_\alpha^\dagger f_\alpha - n_r = 1. \quad (6.6)$$

Associated with this constraint is the U(1) gauge invariance which is the analog of Eqs. (4.2) and (4.5):

$$f_\alpha \rightarrow f_\alpha e^{i\zeta} \quad , \quad \vartheta \rightarrow \vartheta + \zeta. \quad (6.7)$$

Just as in Section IV, there will be an emergent gauge field A_μ in the effective theory of this model. The constraints in Eq. (6.6) will be Gauss law of this theory.

We can now proceed as in Section IV, and write down an effective continuum U(1) gauge theory which captures the low energy physics of the Hubbard model in Eq. (6.1). The degrees of freedom are the b layer electrons $c_{b\alpha}$, the a layer spinons f_α , and the bosonic rotors

$$b = e^{-i\vartheta}. \quad (6.8)$$

The structure of the terms follows from gauge invariance and the preservation of global symmetries. We obtain the Lagrangian density

$$\begin{aligned} \mathcal{L} &= \mathcal{L}_f + \mathcal{L}_b + \mathcal{L}_c \\ \mathcal{L}_f &= f_\alpha^\dagger \left[\frac{\partial}{\partial \tau} + \epsilon_f - iA_\tau - \frac{1}{2m_f} (\nabla - i\mathbf{A})^2 \right] f_\alpha \\ \mathcal{L}_b &= \left[(\partial_\mu - (\epsilon_b - \mu)\delta_{\mu\tau} - iA_\mu + iA_{\text{ext},\mu}) b^\dagger \right] \\ &\quad \times \left[(\partial_\mu + (\epsilon_b - \mu)\delta_{\mu\tau} + iA_\mu - iA_{\text{ext},\mu}) b \right] + s|b|^2 + u|b|^4 \\ \mathcal{L}_c &= c_{b\alpha}^\dagger \left[\frac{\partial}{\partial \tau} - \mu - iA_{\text{ext},\tau} - \frac{1}{2m_c} (\nabla - i\mathbf{A}_{\text{ext}})^2 \right] c_{b\alpha} \\ &\quad - w \left(c_{b\alpha}^\dagger b f_\alpha + b^\dagger f_\alpha^\dagger c_{b\alpha} \right) \end{aligned} \quad (6.9)$$

Here $A_\mu = (A_\tau, \mathbf{A})$ is an emergent U(1) gauge field; we have also introduced a non-fluctuating electromagnetic gauge field $A_{\text{ext},\mu}$ as a source term which couples to the current of the globally conserved electromagnetic charge; we have coarse-grained b to a complex scalar field with both amplitude and phase fluctuations; the symbol μ refers separately to the chemical potential and spacetime component, and the interpretation should be clear from the context; the final Yukawa term is allowed by the symmetries, and represents the inter-layer tunneling w ; the on-site energies ϵ_f and ϵ_b are related to ϵ_a and ϵ_b and have to be tuned so that the system obeys the density constraints to be discussed below.

To review, the continuum theory in Eq. (6.9) has a $\text{U}(1) \times \text{U}(1)_{\text{ext}}$ symmetry associated

with the transformations

$$\begin{aligned} f_\alpha &\rightarrow f_\alpha e^{i\zeta} \quad , \quad b \rightarrow b^{-i\zeta} \quad , \quad c_{b\alpha} \rightarrow c_{b\alpha} \\ f_\alpha &\rightarrow f_\alpha \quad , \quad b \rightarrow b^{i\tilde{\zeta}} \quad , \quad c_{b\alpha} \rightarrow c_{b\alpha} e^{i\tilde{\zeta}} \end{aligned} \quad (6.10)$$

The first U(1) symmetry is gauged by the dynamical emergent U(1) gauge field A_μ . The second U(1) symmetry remains global; the fixed external electromagnetic field $A_{\text{ext},\mu}$ couples a source term which gauges this global symmetry.

In general, there will be 2 Luttinger constraints associated with these two U(1) symmetries⁵³ (as before, we are ignoring spin rotation symmetries here, which is assumed to be always fully preserved). The first transformation in Eq. (6.10) leads to the Luttinger constraint (which is the continuum analog of Eq. (6.6))

$$\sum_\alpha \langle f_\alpha^\dagger f_\alpha \rangle - \langle \mathcal{Q}_b \rangle = \frac{\mathcal{A}_1}{2\pi^2} = \mathcal{N}_a. \quad (6.11)$$

Here \mathcal{N}_a is the density of electrons on layer a in the projected Hilbert space: our present lattice derivation was for $\mathcal{N}_a = 1$, but the continuum theory in Eq. (6.9) is sensible for any value of \mathcal{N}_a . The operator \mathcal{Q}_b is the rotor angular momentum, given by

$$\mathcal{Q}_b = \frac{\partial \mathcal{L}_b}{\partial \mu}. \quad (6.12)$$

Similarly, the second transformation of Eq. (6.6) leads to the constraint

$$\sum_\alpha \langle c_{b\alpha}^\dagger c_{b\alpha} \rangle + \langle \mathcal{Q}_b \rangle = \frac{\mathcal{A}_2}{2\pi^2} = \mathcal{N} - \mathcal{N}_a. \quad (6.13)$$

Thus our analysis so far appears to imply that there must be at least 2 Fermi surfaces, and their areas are constrained by the two independent relations in Eq. (6.11).

This last conclusion seems rather surprising from our earlier discussion of the FL phase. There we found only a single constraint in Eq. (6.3) for the total areas of one or more Fermi surfaces. The only possible conclusion is that the FL phase is *not* one in which the $\text{U}(1) \times \text{U}(1)_{\text{ext}}$ symmetry of the Lagrangian \mathcal{L} in Eq. (6.9) remains unbroken. Rather the FL phase is realized as a Higgs phase in which the $\text{U}(1) \times \text{U}(1)_{\text{ext}}$ symmetry in Eq. (6.10) is broken down to a diagonal U(1). This is the Higgs phase in which the boson b condenses

$$\langle b \rangle \neq 0 \text{ in the FL phase.} \quad (6.14)$$

Once the symmetry is broken in this manner, the corresponding Luttinger constraint no longer applies⁵³. Only the *sum* of the constraints in Eqs. (6.11) and (6.13) applies, and this leads immediately to the defining relation in Eq. (6.3) of the FL phase. The condensation

of b also quenches the emergent $U(1)$ gauge field, so there are no gapless gauge excitations in the FL state, as expected.

We now see that state of the theory \mathcal{L} in which the Luttinger constraints in Eqs. (6.11) and (6.13) apply separately is a new phase: this is the advertised FL^* phase, in which the boson b is uncondensed^{2,3}

$$\langle b \rangle = 0 \text{ in the } FL^* \text{ phase.} \quad (6.15)$$

The full $U(1) \times U(1)_{\text{ext}}$ symmetry is preserved, and the gauge boson A_μ becomes an emergent gapless photon.

However, before accepting this FL^* state as a stable phase of \mathcal{L} , we also have to examine the influence of monopoles in A_μ gauge field, as we did in earlier Section IV. Here the f_α fermions carry the A_μ gauge charge, and these fermions form the \mathcal{A}_1 Fermi surface. This is a crucial difference from Section IV, where the ψ_\pm fermions were gapped. In Section IV we found that the monopoles proliferated, leading to confinement and VBS order. Here, the gapless fermionic excitations at the \mathcal{A}_1 Fermi surface prevent the proliferation of monopoles: the low energy fermions suppress the tunneling event associated with global change in A_μ flux^{58,59}. Thus the emergent $U(1)$ gauge fields remains in an deconfined phase, and the FL^* state is stable. These gapless gauge excitations have strong interactions with the f_α fermions, and this leads to strong critical damping of the fermions at the \mathcal{A}_1 Fermi surface which is described by a strongly-coupled field theory^{60–62}. In contrast, the fermions at the \mathcal{A}_2 Fermi surface are neutral with respect to A_μ , and so their damping is less severe.

The criteria in Eqs. (6.14) and (6.15) show that the transition between the FL and FL^* states is tuned by varying the coupling s in \mathcal{L}_b from negative to positive values. The transition between these phases occurs at a quantum critical point where the scalar b is also critical.

A. Connections to holographic metals

We now connect the above generic theory of the compressible FL and FL^* phases of the Hubbard model to recent studies of compressible metallic phases via the AdS/CFT correspondence.

A connection was made in Ref. 4 between a mean-field solution of models like the Hubbard model in Eq. (6.1) and a particular AdS realization of a holographic metal. Specifically, the bilayer Hubbard model has been solved in a limit with infinite-range hopping matrix elements between the sites (in contrast to the nearest-neighbor hopping shown in Eq. (6.1)). A detailed correspondence was found between the low energy properties of the FL^* phase of such a model and the holographic theory^{63–65} in which the low energy limit factorized to a $AdS_2 \times R^d$ geometry (d is the dimensionality of space). This work has been recently reviewed by the author in a separate article¹.

However, the mean-field solution of Eq. (6.1) and the $AdS_2 \times R^d$ geometry share a number

of artifacts: they have a non-zero ground state entropy, and the spin correlations of layer a scale with dynamic exponent $z = \infty$. These artifacts are not expected to be properties of the field theory \mathcal{L} in Eq. (6.9).

It is clearly of interest to move beyond the $\text{AdS}_2 \times \mathbb{R}^d$ factorization in the holographic theory, and derive a holographic model which has a closer correspondence with the phases of the field theory in Eq. (6.9). A number of recent theories^{64,66–73} have examined the feedback of the finite density matter on the metric of the AdS space, and found that the AdS_2 horizon disappears at $T = 0$, and is replaced by a metric with a finite value of z . Many physical properties of such holographic metals are similar to those of the field theory in Eq. (6.9), but a detailed correspondence awaits future work.

Next, we turn to the recent work of Nickel and Son^{74,75} on holographic liquids, who examined the structure of non-zero temperature diffusion of a global $U(1)$ charge, and of the emergent zero temperature zero-sound mode in holographic liquids. They argued that the low energy theory had an emergent $U(1)$ gauge field, so that the theory had $U(1)_{\text{global}} \times U(1)_{\text{gauge}}$ symmetry. This is strikingly similar to the $U(1) \times U(1)_{\text{ext}}$ symmetry of Eq. (6.9). Indeed, we can more closely map the low energy theory of the FL phase of Eq. (6.9) to the model proposed by Nickel and Son. In the FL phase, we condense the b boson, and focus on the fluctuations of its phase $b = e^{-i\vartheta}$. Then the effective theory of the FL phase of Eq. (6.9) is

$$\mathcal{L}_{FL} = K (\partial_\mu \vartheta - A_\mu + A_{\text{ext},\mu})^2 + \Pi_f(a_\mu) + \dots \quad (6.16)$$

where Π_f is the effective action obtain after integrating out the f spinons, and the ellipses denotes terms associated with the c_b fermions. The structure of Eq. (6.16) is closely related to Eqs. (6) and (52) of Nickel and Son⁷⁴. It would be interesting to extend the holographic analysis to the deconfined phase where b is not condensed, and test its connection to the FL^* state.

Like Nickel and Son, we can use Eq. (6.16) as a basis of the transport properties of the field theory \mathcal{L} in Eq. (6.9). However, rather than working with Eq. (6.16) let us present the equivalent analysis of Ioffe and Larkin⁷⁶. We can characterize the f_α , b , and $c_{b\alpha}$ components of \mathcal{L} by 3 conductivities σ_f , σ_b , and σ_c which describe their response to $U(1)$ gauge fields. Then, in the presence of electric fields \mathbf{E} and \mathbf{E}_{ext} the respect current responses obtained from \mathcal{L} are

$$\begin{aligned} \mathbf{J}_f &= \sigma_f \mathbf{E} \\ \mathbf{J}_b &= \sigma_b (\mathbf{E}_{\text{ext}} - \mathbf{E}) \\ \mathbf{J}_c &= \sigma_c \mathbf{E}_{\text{ext}}. \end{aligned} \quad (6.17)$$

We now use the equations of motion of the A_μ gauge field to conclude that $\mathbf{J}_b = \mathbf{J}_f$; this

equation is clearly a consequence of Eq. (6.6). From this we obtain

$$\mathbf{E} = \frac{\sigma_b}{\sigma_f + \sigma_b} \mathbf{E}_{\text{ext}}; \quad (6.18)$$

thus application of an external electromagnetic field induces a corresponding internal field. The total electrical current in response to the external field is

$$\mathbf{J}_f + \mathbf{J}_c = \left(\sigma_c + \frac{\sigma_b \sigma_f}{\sigma_b + \sigma_f} \right) \mathbf{E}_{\text{ext}}. \quad (6.19)$$

It remains to compute the values of the conductivities σ_f , σ_b and σ_c in the FL and FL* phases, a task we shall not explore here. The result in Eq. (6.19) is equivalent to the analysis of Nickel and Son for their model. Further theoretical work exploring this connection is clearly of interest.

Acknowledgements

This research was supported by the National Science Foundation under grant DMR-0757145 and by a MURI grant from AFOSR.

-
- ¹ S. Sachdev, “Strange metals and the AdS/CFT correspondence,” J. Stat. Mech. **1011**, P11022 (2011) [arXiv:1010.0682 [cond-mat.str-el]].
 - ² T. Senthil, S. Sachdev, and M. Vojta, “Fractionalized Fermi liquids,” Phys. Rev. Lett. **90**, 216403 (2003) [arXiv:cond-mat/0209144].
 - ³ T. Senthil, M. Vojta, and S. Sachdev, “Weak magnetism and non-Fermi liquids near heavy-fermion critical points,” Phys. Rev. B **69**, 035111 (2004) [arXiv:cond-mat/0305193].
 - ⁴ S. Sachdev, “Holographic metals and the fractionalized Fermi liquid,” Phys. Rev. Lett. **105**, 151602 (2010) [arXiv:1006.3794 [hep-th]].
 - ⁵ M. Neumann, J. Nyéki, B. Cowan, and J. Saunders, “Bilayer ^3He : A Simple Two-Dimensional Heavy-Fermion System with Quantum Criticality,” Science **317**, 1356 (2007).
 - ⁶ C. Cohen-Tannoudji, J. Dupont-Roc, and G. Grynberg, *Atom-Photon Interactions: Basic Processes and Applications*, Complement B₁, Wiley-VCH (1998).
 - ⁷ Z. Y. Meng, T. C. Lang, S. Wessel, F. F. Assaad, and A. Muramatsu, “Quantum spin-liquid emerging in two-dimensional correlated Dirac fermions,” Nature **464**, 847 (2010) [arXiv:1003.5809 [cond-mat.str-el]].
 - ⁸ M. Hermele, “SU(2) gauge theory of the Hubbard model and application to the honeycomb lattice,” Phys. Rev. B **76**, 035125 (2007) [arXiv:cond-mat/0701134].

- ⁹ F. Wang, “Schwinger Boson Mean Field Theories of Spin Liquid States on Honeycomb Lattice: Projective Symmetry Group Analysis and Critical Field Theory,” *Phys. Rev. B* **82**, 024419 (2010) [arXiv:1004.2693 [cond-mat.str-el]].
- ¹⁰ Y. -M. Lu and Y. Ran, “Spin liquids on a honeycomb lattice: Projective Symmetry Group study of Schwinger fermion mean-field theory,” arXiv:1005.4229 [cond-mat.str-el].
- ¹¹ Y. -M. Lu and Y. Ran, “ Z_2 spin liquid and chiral antiferromagnetic phase in Hubbard model on the honeycomb lattice: Duality between Schwinger-fermion and Schwinger-boson representations,” arXiv:1007.3266 [cond-mat.str-el].
- ¹² C. Xu and S. Sachdev, “Majorana liquids: the complete fractionalization of the electron,” *Phys. Rev. Lett.* **105**, 057201 (2010) [arXiv:1004.5431 [cond-mat.str-el]].
- ¹³ C. Xu, “Quantum Spin Hall, triplet Superconductor, and topological liquid on the honeycomb lattice,” arXiv:1010.0455 [cond-mat.str-el].
- ¹⁴ I. F. Herbut, “Interactions and phase transitions on graphene’s honeycomb lattice,” *Phys. Rev. Lett.* **97**, 146401 (2006) [arXiv:cond-mat/0606195].
- ¹⁵ I. F. Herbut, V. Juricic, and B. Roy, “Theory of interacting electrons on the honeycomb lattice,” *Phys. Rev. B* **79**, 085116 (2009) [arXiv:0811.0610 [cond-mat.str-el]].
- ¹⁶ I. F. Herbut, V. Juricic, and O. Vafek, “Relativistic Mott criticality in graphene,” *Phys. Rev. B* **80**, 075432 (2009) [arXiv:0904.1019 [cond-mat.str-el]].
- ¹⁷ S. Sachdev, “Quantum phase transitions of correlated electrons in two dimensions,” *Physica A* **313**, 252 (2002) [arXiv:cond-mat/0109419].
- ¹⁸ S. Sachdev, *Quantum Phase Transitions*, 2nd ed., Cambridge (2011).
- ¹⁹ S. Sachdev, “Non-zero temperature transport near fractional quantum Hall critical points,” *Phys. Rev. B* **57**, 7157 (1998) [arXiv:cond-mat/9709243].
- ²⁰ K. Damle and S. Sachdev, “Non-zero temperature transport near quantum critical points,” *Phys. Rev. B* **56**, 8714 (1997) [arXiv:cond-mat/9705206].
- ²¹ L. Fritz, J. Schmalian, M. Müller and S. Sachdev, “Quantum critical transport in clean graphene,” *Phys. Rev. B* **78**, 085416 (2008) [arXiv:0802.4289 [cond-mat.str-el]].
- ²² M. Müller, L. Fritz, and S. Sachdev, “Quantum critical relativistic magnetotransport in graphene,” *Phys. Rev. B* **78**, 115406 (2008) [arXiv:0805.1413 [cond-mat.str-el]].
- ²³ I. F. Herbut, V. Juricic, and O. Vafek, “Coulomb interaction, ripples, and the minimal conductivity of graphene,” *Phys. Rev. Lett.* **100** 046403 (2008) [arXiv:0707.4171 [cond-mat.mes-hall]].
- ²⁴ V. Juricic, O. Vafek, I. F. Herbut, “Conductivity of interacting massless Dirac particles in graphene: Collisionless regime,” arXiv:1009.3269 [cond-mat.mes-hall].
- ²⁵ C. P. Herzog, P. Kovtun, S. Sachdev and D. T. Son, “Quantum critical transport, duality, and M-theory,” *Phys. Rev. D* **75**, 085020 (2007) [arXiv:hep-th/0701036].
- ²⁶ R. C. Myers, S. Sachdev and A. Singh, “Holographic Quantum Critical Transport without Self-Duality,” arXiv:1010.0443 [hep-th].
- ²⁷ S. Sachdev, X. Yin, “Quantum phase transitions beyond the Landau-Ginzburg paradigm and

- supersymmetry,” *Annals Phys.* **325**, 2 (2010) [arXiv:0808.0191 [cond-mat.str-el]].
- ²⁸ C. Dasgupta and B. I. Halperin, “Phase Transition in a Lattice Model of Superconductivity,” *Phys. Rev. Lett.* **47**, 1556 (1981).
- ²⁹ P. Kovtun, D. T. Son and A. O. Starinets, “Viscosity in strongly interacting quantum field theories from black hole physics,” *Phys. Rev. Lett.* **94**, 111601 (2005) [arXiv:hep-th/0405231].
- ³⁰ M. Müller, J. Schmalian, and L. Fritz, “Graphene - a nearly perfect fluid,” *Phys. Rev. Lett.* **103**, 025301 (2009) [arXiv:0903.4178 [cond-mat.str-el]].
- ³¹ B. I. Shraiman and E. D. Siggia, “Mobile Vacancies in a Quantum Heisenberg Antiferromagnet,” *Phys. Rev. Lett.* **61**, 467 (1988).
- ³² H. J. Schulz, “Effective action for strongly correlated fermions from functional integrals,” *Phys. Rev. Lett.* **65**, 2462 (1990).
- ³³ S. Sachdev, M. A. Metlitski, Y. Qi, and Cenke Xu, “Fluctuating spin density waves in metals,” *Phys. Rev. B* **80**, 155129 (2009) [arXiv:0907.3732 [cond-mat.str-el]].
- ³⁴ A. D’Adda, P. Di Vecchia, and M. Lüscher, “A $1/n$ Expandable Series of Nonlinear Sigma Models with Instantons,” *Nucl. Phys. B* **146**, 63 (1978).
- ³⁵ E. Witten, “Instantons, the Quark Model, and the $1/n$ Expansion,” *Nucl. Phys.* **B149**, 285 (1979).
- ³⁶ N. Read and S. Sachdev, “Spin-Peierls, valence bond solid, and Neel ground states of low dimensional quantum antiferromagnets,” *Phys. Rev. B* **42**, 4568 (1990).
- ³⁷ O. I. Motrunich and A. Vishwanath, “Emergent photons and new transitions in the $O(3)$ sigma model with hedgehog suppression,” *Phys. Rev. B* **70**, 075104 (2004) [arXiv:cond-mat/0311222].
- ³⁸ T. Senthil, A. Vishwanath, L. Balents, S. Sachdev, and M. P. A. Fisher, “Deconfined quantum critical points,” *Science* **303**, 1490 (2004) [arXiv:cond-mat/0311326].
- ³⁹ T. Senthil, L. Balents, S. Sachdev, A. Vishwanath, and M. P. A. Fisher, “Quantum criticality beyond the Landau-Ginzburg-Wilson paradigm,” *Phys. Rev. B* **70**, 144407 (2004) [arXiv:cond-mat/0312617].
- ⁴⁰ A. M. Polyakov, “Compact gauge fields and the infrared catastrophe,” *Phys. Lett. B* **59**, 82 (1975).
- ⁴¹ L. Fu, S. Sachdev, C. Xu, “Geometric phases and competing orders in two dimensions,” arXiv:1010.3745 [cond-mat.str-el].
- ⁴² A. G. Abanov, P. B. Wiegmann, “Theta terms in nonlinear sigma models,” *Nucl. Phys.* **B570**, 685-698 (2000) [arXiv:hep-th/9911025].
- ⁴³ A. Tanaka and Xiao Hu, “Many-body spin Berry phases emerging from the π -flux state: antiferromagnetic/valence-bond-solid competition,” *Phys. Rev. Lett.* **95**, 036402 (2005) [arXiv:cond-mat/0501365].
- ⁴⁴ T. Senthil and M. P. A. Fisher, “Competing orders, non-linear sigma models, and topological terms in quantum magnets,” *Phys. Rev. B* **74**, 064405 (2006) [arXiv:cond-mat/0510459].
- ⁴⁵ H. Yao and D. -H. Lee, “Topological insulators and topological non-linear sigma models,”

- arXiv:1003.2230 [cond-mat.str-el].
- ⁴⁶ R. K. Kaul, Y. B. Kim, S. Sachdev, and T. Senthil, “Algebraic Charge Liquids,” *Nature Physics* **4**, 28 (2008) [arXiv:0706.2187 [cond-mat.str-el]].
 - ⁴⁷ R. K. Kaul, A. Kolezhuk, M. Levin, S. Sachdev, and T. Senthil, “Hole dynamics in an antiferromagnet across a deconfined quantum critical point,” *Phys. Rev. B* **75**, 235122 (2007) [arXiv:cond-mat/0702119].
 - ⁴⁸ Y. Qi and S. Sachdev, “Effective theory of Fermi pockets in fluctuating antiferromagnets,” *Phys. Rev. B* **81**, 115129 (2010) [arXiv:0912.0943 [cond-mat.str-el]].
 - ⁴⁹ E. G. Moon, S. Sachdev, “The underdoped cuprates as fractionalized Fermi liquids: transition to superconductivity,” arXiv:1010.4567 [cond-mat.str-el].
 - ⁵⁰ T. C. Ribeiro and X.-G. Wen, “Doped carrier formulation and mean-field theory of the t - t' - t'' - J model,” *Phys. Rev. B* **74**, 155113 (2006) [arXiv:0705.2261 [cond-mat.str-el]].
 - ⁵¹ Ying Ran and X.-G. Wen, “Dichotomy in underdoped high T_c superconductors and spinon-dopon approach to t - t' - t'' - J model,” arXiv:cond-mat/0611034.
 - ⁵² T. C. Ribeiro and X.-G. Wen, “Electromagnetic response of high- T_c superconductors – the slave-boson and doped-carrier theories,” *Phys. Rev. B* **77**, 144526 (2007) [arXiv:0705.2261 [cond-mat.str-el]].
 - ⁵³ S. Powell, S. Sachdev, and H. P. Büchler, “Depletion of the Bose-Einstein condensate in Bose-Fermi mixtures,” *Phys. Rev. B* **72**, 024534 (2005) [arXiv:cond-mat/0502299].
 - ⁵⁴ O. I. Motrunich, “Variational study of triangular lattice spin-1/2 model with ring exchanges and spin liquid state in κ -(ET) $_2$ Cu $_2$ (CN) $_3$,” *Phys. Rev. B* **72**, 045105 (2005) [arXiv:cond-mat/0412556].
 - ⁵⁵ S.-S. Lee and P. A. Lee, “U(1) Gauge Theory of the Hubbard Model : Spin Liquid States and Possible Application to κ -(BEDT-TTF) $_2$ Cu $_2$ (CN) $_3$,” *Phys. Rev. Lett.* **95**, 036403 (2005) [arXiv:cond-mat/0502139].
 - ⁵⁶ W. Rantner and X.-G. Wen, “Electron spectral function and algebraic spin liquid for the normal state of underdoped high T_c superconductors,” *Phys. Rev. Lett.* **86**, 3871 (2001) [arXiv:cond-mat/0010378].
 - ⁵⁷ S. Florens and A. Georges, “Slave-rotor mean field theories of strongly correlated systems and the Mott transition in finite dimensions,” *Phys. Rev. B* **70**, 035114 (2004) [arXiv:cond-mat/0404334].
 - ⁵⁸ M. Hermele, T. Senthil, M. P. A. Fisher, P. A. Lee, N. Nagaosa, and X.-G. Wen, “On the stability of U(1) spin liquids in two dimensions,” *Phys. Rev. B* **70**, 214437 (2004) [arXiv:cond-mat/0404751].
 - ⁵⁹ Sung-Sik Lee, “Stability of the U(1) spin liquid with spinon Fermi surface in 2+1 dimensions,” *Phys. Rev. B* **78**, 085129 (2008) [arXiv:0804.3800 [cond-mat.str-el]].
 - ⁶⁰ Sung-Sik Lee, “Low energy effective theory of Fermi surface coupled with U(1) gauge field in 2+1 dimensions,” *Phys. Rev. B* **80**, 165102 (2009) [arXiv:0905.4532 [cond-mat.str-el]].

- ⁶¹ M. A. Metlitski, and S. Sachdev, “Quantum phase transitions of metals in two spatial dimensions: I. Ising-nematic order,” *Phys. Rev.* **B82**, 075127 (2010) [arXiv:1001.1153 [cond-mat.str-el]].
- ⁶² D. F. Mross, J. McGreevy, H. Liu, and T. Senthil, “A controlled expansion for certain non-Fermi liquid metals,” arXiv:1003.0894 [cond-mat.str-el].
- ⁶³ T. Faulkner, H. Liu, J. McGreevy, and D. Vegh, “Emergent quantum criticality, Fermi surfaces, and AdS(2),” arXiv:0907.2694 [hep-th].
- ⁶⁴ T. Faulkner and J. Polchinski, “Semi-Holographic Fermi Liquids,” arXiv:1001.5049 [hep-th].
- ⁶⁵ S. Kachru, A. Karch, and S. Yaida, “Holographic Lattices, Dimers, and Glasses,” *Phys. Rev.* **D81**, 026007 (2010) [arXiv:0909.2639 [hep-th]].
- ⁶⁶ S. A. Hartnoll, J. Polchinski, E. Silverstein, and D. Tong, “Towards strange metallic holography,” *JHEP* **1004**, 120 (2010) [arXiv:0912.1061 [hep-th]].
- ⁶⁷ C. Charmousis, B. Gouteraux, B. S. Kim, E. Kiritsis, and R. Meyer, “Effective Holographic Theories for low-temperature condensed matter systems,” arXiv:1005.4690 [hep-th].
- ⁶⁸ S. A. Hartnoll and A. Tavanfar, “Electron stars for holographic metallic criticality,” arXiv:1008.2828 [hep-th].
- ⁶⁹ S. A. Hartnoll, D. M. Hofman, and A. Tavanfar, “Holographically smeared Fermi surface: Quantum oscillations and Luttinger count in electron stars,” arXiv:1011.2502 [hep-th].
- ⁷⁰ X. Arsiwalla, J. de Boer, K. Papadodimas, and E. Verlinde, “Degenerate Stars and Gravitational Collapse in AdS/CFT,” arXiv:1010.5784 [hep-th].
- ⁷¹ K. Goldstein, S. Kachru, S. Prakash, and S. P. Trivedi, “Holography of Charged Dilaton Black Holes,” *JHEP* **1008**, 078 (2010) [arXiv:0911.3586 [hep-th]].
- ⁷² K. Goldstein, N. Iizuka, S. Kachru, S. Prakash, S. P. Trivedi, and A. Westphal, “Holography of Dyonic Dilaton Black Branes,” *JHEP* **1010**, 027 (2010) [arXiv:1007.2490 [hep-th]].
- ⁷³ S. Kachru, A. Karch, and S. Yaida, “Adventures in Holographic Dimer Models,” arXiv:1009.3268 [hep-th].
- ⁷⁴ D. Nickel and D. T. Son, “Deconstructing holographic liquids,” arXiv:1009.3094 [hep-th].
- ⁷⁵ A. Karch, D. T. Son, and A. O. Starinets, “Holographic Quantum Liquid,” *Phys. Rev. Lett.* **102**, 051602 (2009) [arXiv:0806.3796 [hep-th]].
- ⁷⁶ L. B. Ioffe and A. I. Larkin, “Gapless fermions and gauge fields in dielectrics,” *Phys. Rev. B* **39**, 8988 (1989).